DEVELOPMENT OF LEAD FOAMS FOR AUTOMOBILE BATTERIES

A Thesis Submitted to
the Graduate School of Engineering and Sciences of
İzmir Institute of Technology
in Partial Fulfillment of the Requirements for the Degree of

MASTER OF SCIENCE

in Materials Science and Engineering

by
Umut SAVACI

July 2012
İZMİR

We approve the thesis of **Umut SAVACI**

Examining Committee Members:

Prof. Dr. Mustafa GÜDEN
Department of Mechanical Engineering
İzmir Institute of Technology

Prof. Dr. Muhsin ÇİFTÇİOĞLU
Department of Chemical Engineering
İzmir Institute of Technology

Assoc. Prof. Dr. Mustafa M. DEMİR
Department of Chemistry
İzmir Institute of Technology

03 July 2012

Prof. Dr. Mustafa GÜDEN
Supervisor, Department of Mechanical Engineering
İzmir Institute of Technology

Assoc. Prof. Dr. Alper TAŞDEMİRCİ
Co-Supervisor, Department of Mechanical Engineering
İzmir Institute of Technology

Assoc. Prof. Dr. Mustafa M. DEMİR
Head of the Department of Materials Science and Engineering

Prof. Dr. R. Tuğrul SENGER
Dean of the Graduate School of Engineering and Sciences

ACKNOWLEDGEMENTS

I am grateful to my advisor, Prof. Dr. Mustafa Güden and my co-advisor Associate. Prof. Dr. Alper Taşdemirci, for their supervision, guidance, support and motivation from the beginning to the final stage, enabled to me to completely understand the subject. I also thank to Dr. Sinan Yılmaz, from İNCİ Akü, for his material and technical support during this study. I would like to thank to the team of IZTECH Materials Research Center (IYTE-MAM) for their assistance.

I gratefully thank to my colleagues, Yiğit Attila, Doğuş Zeren, Kutlay Odacı, Ali Kara, Cenk Kılıçaslan, and Ali Kıvanç Turan for their supports and helps. I also wish to thank my family who deserve a special mention for their endless support. And finally, I would like to express my special thanks to my girlfriend Yonca Koncalıoğlu for her encouragement, support and patience during this graduate work.

ABSTRACT

DEVELOPMENT OF LEAD FOAMS FOR AUTOMOBILE BATTERIES

Open cell lead foam samples with, 48, 55, 60, 65 and 74% porosity, were successfully prepared by powder metallurgy and casting using ammonium bicarbonate, silica beads and salt particles as space holder filler. Additionally electrowinning and powder compact foaming methods were tried. The resulting foam samples resembled open foam cell structure; each cell had interconnections with neighboring cells. Small size lead (II) fluoride precipitates were observed interior of cells in the foam samples prepared using silica beads, resulting from the reaction between silica and HF acid during space holder removal. The compression stress-strain curve of foam samples prepared by powder metallurgy showed a brittle behavior following the initial elastic, while foam samples prepared by casting showed elastic-plastic characteristic metal foam deformation; crushing of cell edges on the bent cell walls and tearing of thin cell walls. The collapse stresses of the prepared foams were fitted with scaling relations. The imperfections such as curved, wrinkled and missing cell walls, voids on the cell edges and cell walls and non-uniform density lead to discrepancy between experimental and theoretical scaling parameters.

ÖZET

OTOMOBİL AKÜLERİ İÇİN KURŞUN KÖPÜK GELİŞTİRİLMESİ

Hacimce %48, 55, 60, 65 ve 74 oranlarında por içeren açık hücreye sahip kurşun köpük örnekleri amonyum bikarbonat hacim tutucu partikülleri kullanılarak toz metalurjisi, tuz ve silika bilya hacim tutucu partikülleri kullanılarak döküm metodu vasıtasıyla başarıyla üretilmiştir. Ayrıca ek olarak elektroliz ile geri kazanım ve toz kompaktların köpürtülmesi metodları da denenmiştir. Elde edilen köpük örnekleri açık hücreli köpük yapısına benzemektedir; yapıdaki her hücre diğer komşu hücreler ile bağlantılıdır. Kurşun ve hidroflorik asitin hacim tutucu partiküllerin yapıdan uzaklaştırılması esnasında meydana gelen reaksiyonu sonucunda silika bilya kullanılarak elde edilmiş köpük yapılarında küçük boyutlu kurşun florür çökeltilerinin hücre duvarlarında oluştuğu gözlemlenmiştir. Basma gerinme-gerilme test sonuçlarına göre toz metalurjisi ile üretilen köpüklerin kırılgan davranış sergilediği gözlemlenirken, döküm metodu ile üretilen köpüklerin karakteristik elastik-plastik davranış, hücre kenarlarının hücre duvarları üzerine kırılması ve ince hücre duvarlarının yırtılması, gösterdiği görülmüştür. Testler sonucunda elde edilen çökme gerinmesi değerleri ölçekleme denklemleri kullanılarak ölçekleme katsayıları hesaplanmıştır. Yapıda bulunan katlanmış, eğri ve eksik hücre duvarları, hücre kenar ve duvarlarındaki boşluklar ve homojen olmayan kurşun yoğunluğu gibi süreksizlikler sebebi ile teorik ve deneysel ölçekleme katsayıları arasında farklılık olduğu görülmüştür.

TABLE OF CONTENTS

LIST OF FIGURES

Figure **Page**

LIST OF TABLES

Table **Page**

CHAPTER 1

INTRODUCTION

Cellular materials, natural or man-made, are relatively well-known and commonly used in our daily life as insulation, packaging and filtration materials. A cellular material is literally defined as the assembly of cells with solid edges or faces packed together to fill the space [1]. Solid edges or faces provide interconnected network of the edge material, and this network contains the air inside. The cellular materials are very common in nature, for example bone, wood, cork and sponges. Understanding the advantages of cellular materials gives an inspiration to mankind to produce their synthetic-or man-made- cellular structures using various different materials. Initially, the cellular materials were made of polymers; however, with the development of novel processing techniques, new types of cellular materials based on metals, ceramics and glasses were produced. Foams offer lightweight for structural and functional applications. Based on the application area, the structure could be modified in order to obtain open or closed pores by selecting appropriate production method. In open cell foams, the cells are connected merely by struts, which allow the penetration of fluid media like liquids or gases. However, in closed cell foams, the cells are isolated with the cell walls; there is no interconnection between the pores.

The lead-acid batteries are the most important type of rechargeable batteries because of their low costs and moderate performances. Today, the environmental pollution increases day by day and the efforts to decline pollution has become paramount importance. The major cause of the environmental pollution is the exhaust emissions from the internal combustion engines. This problem drives the automotive industry to produce new, environmentally friendly vehicles, including hybrid-electric and electric vehicles. However, these new types of cars require better batteries that provide higher power output and higher capacity to power up the electric motors for higher mileages. Therefore, conventional batteries do not satisfy the energy requirements of future vehicles. This trend has naturally pushed battery industry to develop new types of batteries including the most popular and well-known Li-ion batteries. Lead-acid batteries are still the ultimate choice for the vehicles at present as

they have relatively low production costs, ease of production and recyclability. On the other side, the conventional lead-acid batteries have several disadvantages: low capacities, low powers, short period of cycle life and heavy weight. A typical lead-acid car battery is as heavy as 14 kilograms; lead electrodes constitute about 21% of total weight. One way of reducing the weight of currently used lead-acid batteries is to replace the heavy lead electrodes with low density porous lead electrodes.

In recent years, the production of lead foam has taken the attention of the battery producers. The use of porous lead electrodes leads to lower density, higher surface area, higher utilization efficiency and higher discharge density [2-4]. The increase in electrode surface area and the reduction in electrode mass increase the utilization efficiency of positive active material up to 50% which is much higher than the conventional grid electrode [5]. Basically, the use of lead foam in batteries provides the same performance with lower volume (or weight) or higher performance with the same volume (or weight). The lead foams use in lead-acid batteries may open the way of new applications. For example, they can be used in submarines in which every kg or cm^3 has critical importance.

The ultimate goal of this thesis is to investigate the potential methods of lead foam processing routes which can be used in processing lead electrodes in lead-acid batteries.

CHAPTER 2

LEAD-ACID BATTERIES

2.1. Batteries

The electrical energy has an important role in daily life since the electronic and electrical devices have become fundamental part of modern life. The electrical energy or electricity cannot be stored directly; therefore, the storage of the electricity is a prime problem with the utilization of the electrical energy. The electricity is stored conventionally by means of batteries. A battery can store the electrical energy simply by converting electric energy into chemical energy or vice versa. The conversion of is accomplished through electrochemical oxidation-reduction reactions. The electrochemical reaction is the electron transfer between electronic conductor and some species in an electrolytic phase. For the rechargeable batteries, charging is done by means of the reversal of the discharge (redox) reactions. The electrochemical reactions involve the transportation of electrons from one material to another with an electric circuit.

A battery consists of the electrochemical units known as electrolytic cell. The electrolytic cells are connected by serial or parallel to each other to adjust the output voltage and capacity. These individual cells consist of three main parts; anode, cathode and an electrolyte. The parts and reactions of the parts are explained below.

Anode is the negative electrode of the cell which is also known as oxidizing electrode. This electrode provides electrons to the electrical circuit and oxidizes during electrochemical reactions. The reaction at the anode is as follows:

$$M \rightarrow M^{n+} + ne^{-} \qquad (2.1)$$

here M is a metal and n is the number of electrons.

Cathode is the positive electrode of the cell and accepts the electrons during discharge state. At the positive electrode following reaction takes place

$$nX + ne^- \rightarrow nX^- \quad (2.2)$$

here X is an reducing agent.

Electrolyte provides the medium for ion transfer between the anode and cathode. The electrolyte is usually a liquid composing of acids or alkalis to provide ionic conductivity. The acid solutions diluted with water gives positive ions (H^+). The main characteristic of the electrolyte is the low resistance as the electronic current flow is limited by the transportation of ions.

A battery should satisfy two requirements: it should be light-weight and high cell voltage and capacity. The anode material is selected among the materials that provide high efficiency as a reducing agent, high coulombic output (Ah/g), high conductivity and stability at low cost. Generally metals, such as lead (Pb), zinc (Zn), lithium (Li) and their alloys are used as the anode material. The cathode material must be a good oxidizing agent, stable in electrolyte solution, and provide appropriate working voltage. The most commonly used cathode materials include metal oxides like lead oxide (PbO_2) and nickel (III) oxide (NiOOH). The electrolyte should have high ionic conductivity but not high electrical conductivity, since the electrical conductivity causes internal short circuit. The electrolyte should also be inert to electrodes and plastic casing; hence, causing no reactions taking place between electrolyte and battery parts. The most frequently used electrolytes are aqueous solutions but also non-aqueous electrolytes are used in special batteries. The anode and cathode are covered with a membrane or microporous envelope and separated with plastic spacers to prevent the physical short circuiting. The membrane should provide the desired ionic conductivity.

The batteries are classified into two groups: primary and secondary. Primary batteries are the non-rechargeable batteries. These batteries are discharged only once as the electrochemical reaction is irreversible. They are generally inexpensive and useful for the portable applications due to the lightweight and low cost. The most commonly used primary batteries are lithium, zinc-carbon, magnesium and aluminum batteries. Figure 2.1(a) and (b) show the cross section views of lithium and zinc-carbon batteries, respectively.

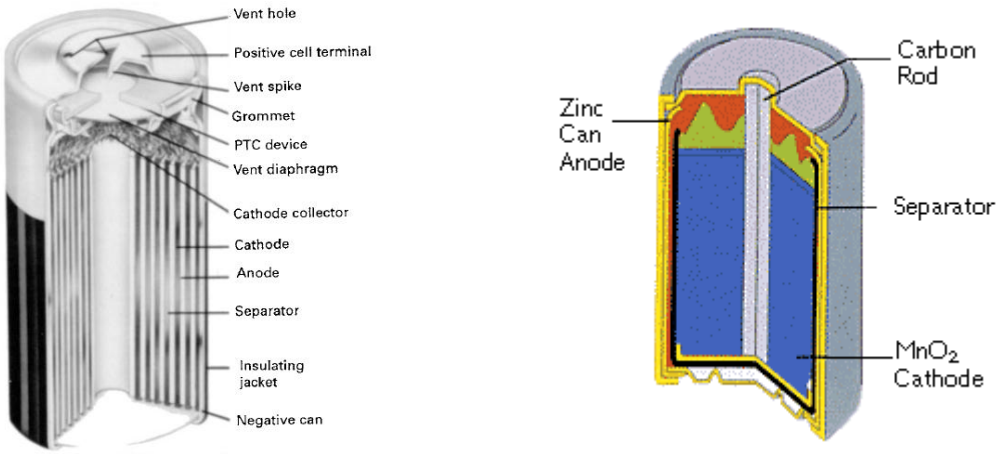

(a) (b)

Figure 2.1. Cross-section view of (a) a lithium [6] and (b) a zinc-carbon [7] batteries.

Secondary batteries are rechargeable; the externally applied electrical energy forces the electrochemical reaction to proceed in the reverse of discharge. These batteries provide advantageous such as high power density, high discharge rate, good cryogenic performance, but their energy densities are generally lower than those of the primary batteries. Applications include starting, lightning and ignition in automobiles, emergency power sources, hybrid electric vehicles and stationary energy storages. Figure 2.2(a) and (b) show the cross sections of a nickel metal hybrid (NiMH) and a lead acid battery, respectively.

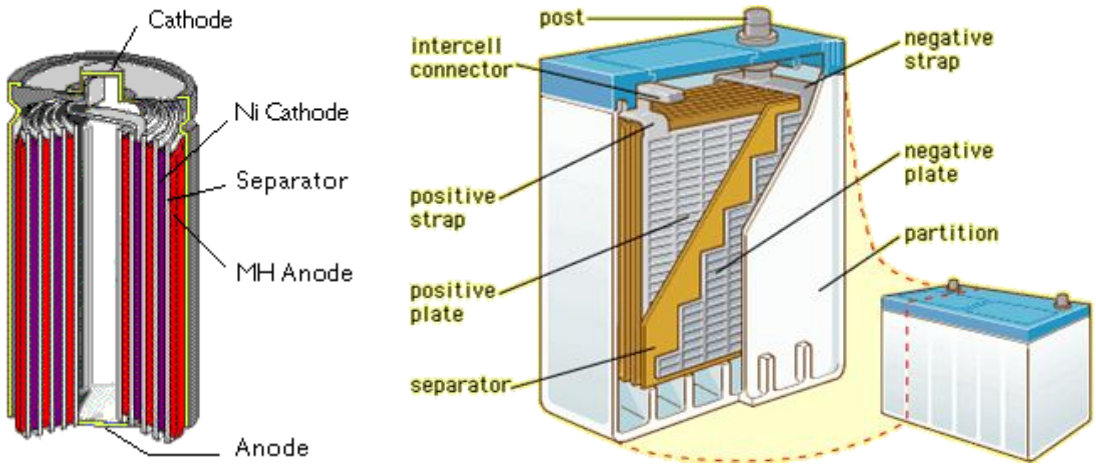

(a) (b)

Figure 2.2. Cross section view of (a) NiMH [7] and (b) lead acid [8] batteries.

The lead-acid batteries are the most widely used secondary battery invented in 1859. Because of their advantages, such as, ease of fabrication, low cost, easy of

processing in various sizes and capacities, and ease of recycling of cell components. Lead-acid batteries have been used for over 100 years. The production and the use continue to grow with new application areas such as energy storage and electric and hybrid vehicles. Also with the increasing production numbers of current vehicles the use of lead-acid batteries will increase.

2.2. Lead-Acid Battery

The electrochemical reactions of discharge and charge states are sequentially shown in Figures 2.3(a) and (b). In discharge state the electrons flow from cathode to anode as seen in Figure 2.3(a). While, the electrons flow from anode to cathode in the charge state as depicted in Figure 2.3(b). During discharge, the anode is oxidized; in other words, it gives electrons and the cathode is reduced, accepting electrons. The circuit is completed with the flows of anions (negative ions) and cations (positive ions) to the anode and cathode, respectively. During charging of a rechargeable battery, the oxidation (anodic) and the reduction (cathodic) reactions occur in positive and negative electrodes, respectively.

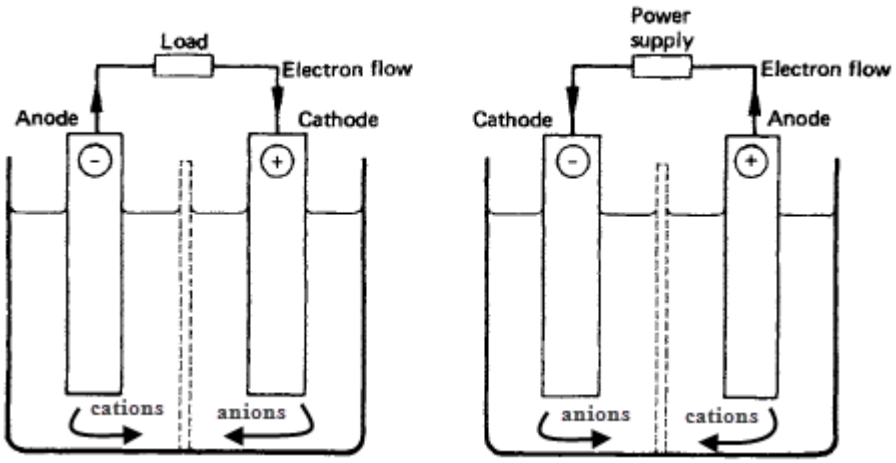

(a) (b)

Figure 2.3. Electrochemical reactions in a cell during (a) discharge and (b) charge states [9].

In lead-acid battery, the metallic lead is used as the negative electrode. The positive electrode is highly conductive lead dioxide. Both electrodes are immersed in electrode solution, a 37 wt% diluted sulfuric acid (H_2SO_4) solution. During discharge,

sulfuric acid is consumed by the production of water as by product. Lead sulfate ($PbSO_4$) is produced with additional dissolution-precipitation reactions at both negative and positive electrodes. During discharge, the following reactions take place:

Negative electrode: $Pb \rightarrow Pb^{2+} + 2e$

$Pb^{2+} + SO_4^{2-} \rightarrow PbSO_4$ $\quad E^o = -0.358$ V

$2H^+ + 2e^- \rightarrow H_2$

Positive electrode: $PbO_2 + 4H^+ + 2e^- \rightarrow Pb^{2+} + 2H_2O$

$Pb^{2+} + SO_4^{2-} \rightarrow PbSO$ $\quad E^o = +1.690$ V

$H_2O + 2e^- \rightarrow ½\ O_2 + 2H^+$

Overall reaction: $Pb + PbO_2 + 2H_2SO_4 \rightarrow 2PbSO_4 + 2H_2O$

$V^o = +2.048$ V

$H_2O \rightarrow H_2 + ½\ O_2$

where, E^o and V^o is the standard electrode potential for each cell reaction and standard cell voltage, respectively. The standard cell voltage means that one cell provides theoretically 2.048 V. The overall voltage of the battery can be multiplied by 2, 6, 12, 24, and 36 V by connecting the cells serially. During charging with an electric source, the reactions given above proceed in the reverse direction.

2.3. Properties of Batteries

There are different types of batteries used in numerous applications. The battery selection is the key for a suitable application. In certain applications, for example for a guided rocket, high output primary batteries are better suited than secondary batteries. The selection of the battery must be done based on the specifications. Most important properties of batteries are the theoretical capacity, theoretical voltage, energy density, specific energy, specific power, current density and power density. Table 2.1 tabulates the properties of commonly used primary and secondary batteries. The properties of batteries are standardized. There are few standards on the batteries such as U.S. national (ANSI, MIL) and international (IEC) standards. These standards specify the properties and also dimensions of each part of the battery (case, electrodes, connection fuses). IEC 60095 and MIL-B-11188 are the standards used for lead acid batteries.

Table 2.1. Properties of the selected primary and secondary batteries [6].

	Battery type	Anode	Cathode	Theoretical values			
				V	g/Ah	Ah/kg	Wh/kg
Primary Batteries	Leclanché	Zn	MnO_2	1.6	4.46	224	358
	Magnesium	Mg	MnO_2	2.8	3.69	271	759
	Alkaline	Zn	MnO_2	1.5	4.46	224	358
	Silver Oxide	Zn	Ag_2O	1.6	5.55	180	288
	$Li/SOCl_2$	Li	$SOCl_2$	3.65	3.25	403	1471
Secondary Batteries	Lead-acid	Pb	PbO_2	2.1	8.32	120	252
	Nickel-cadmium	Cd	Ni oxide	1.35	5.52	181	244
	Nickel-metal hybride	MH	Ni oxide	1.35	5.63	178	240
	Lithium-ion	LiC_6	$LiCoO_2$	4.1	9.98	100	410

2.3.1. Theoretical Capacity

Theoretical capacity known as coulombic capacity is function of anode and cathode materials. Capacity is determined by the amount of active materials in the cell and expressed as the quantity of electricity involved in the electrochemical reaction. The unit of the capacity is expressed in terms of coulombs or ampere-hour (Ah). It is calculated from the equivalent weight of the reactants in the electrochemical reaction (Ah/g). Practical meaning of the capacity is the discharge time of the battery based on the discharge current. For example, the battery having 300 Ah capacity, provides 100 A for 3 h [6].

2.3.2. Theoretical Voltage

The potential of a cell depends on the type of active materials in the cell and is calculated from the electrode potentials using the following equation:

Anode (oxidation potential) + Cathode (reduction potential) = Standard cell potential

2.3.3. Theoretical, Specific Energy and Energy Density

The capacity of cell can also be expressed as energy by considering voltage and capacity. Theoretical energy is the maximum energy for a specific electrochemical cell and calculated as

$$\text{Watt-hour (Wh)} = \text{Voltage (V)} \times \text{Ampere-hour (Ah)}$$

Specific energy is the watt-hour capacity per gram of active material. It is expressed as Wh/kg. Specific energy can also be expressed as energy density on the basis of volume (Wh/L).

2.3.4. Current and Power Density

Current density is the amount of current that is provided by the per unit area of electrode and usually expressed as milliamperes per cm^2 (mA/cm^2). Power density is the expression for the energy (watts) output of battery for a given volume or weight (W/L or W/kg).

CHAPTER 3

PROCESSING AND CHARACTERIZATION OF CELLULAR METALS

3.1. Production Methods for Cellular Metals

Different methods are used to manufacture cellular metals. In few of these methods, similar techniques are used for foaming of polymeric liquids, whereas others are specially designed by taking advantage of the characteristic properties of metals. The properties of foam metals and other cellular metals depend on the properties of the metal from which they are made, the relative density and the cell topology (open or closed cell), size and shape. Properties of the foam metals can be tailored by choosing an appropriate processing technique which affects the cell topology and relative density of the finished foam product. The production methods are divided into three categories based on the physical state of the metal processed; liquid state, solid state and deposition. Some of these production methods provide open cell foams while others provide closed cell foams.

3.1.1. Liquid State Processing of Cellular Metals

In the first group of processing methods, the cellular structure is formed from the molten metal. These methods are direct foaming, indirect foaming via polymer foam or casting a liquid metal around space holding material.

3.1.1.1 Direct Foaming of Metals

Metallic foams are produced directly by injecting a gas from an external source into liquid metal to form gas bubbles or addition of in-situ gas releasing blowing agents to the melt. The foaming by gas injection is commercialized by the Cymat/Hydro [10] metallic foam casting process. Low density Al foams are continuously processed using

this method. The schematic of the gas injection process is shown in Figure 3.1. In the first part of the foam production with this method reinforcing oxide or carbide ceramic particles are added into the metal melt. The inclusion of reinforcing ceramic particles increases the viscosity of the melt and stabilizes the air bubbles inside the melt by retarding drainage. Typically air and inert gases like argon are injected into molten metal by using rotating impellers and vibrating nozzles. The size of the bubbles is controlled by the gas flow rate, the impeller design and speed of impeller. By using this method up to 98% porous closed cell metal foams are produced.

In the second method, blowing agent materials are added into the melt directly. The blowing agent decomposes with heat and releases gas and creates bubbles inside the melt. Typical blowing agents used include TiH_2, ZrH_2 and $CaCO_3$. The blowing agent is added to a liquid alloy just above melting temperature of the alloy but below the decomposition temperature of the blowing agent. Al foams known as Alporas foams are currently commercially produced using this method [11]. The schematic of the Alporas Al foam production method is shown in Figure 3.2. The molten metal is thickened by Ca addition, before the addition of blowing agent.

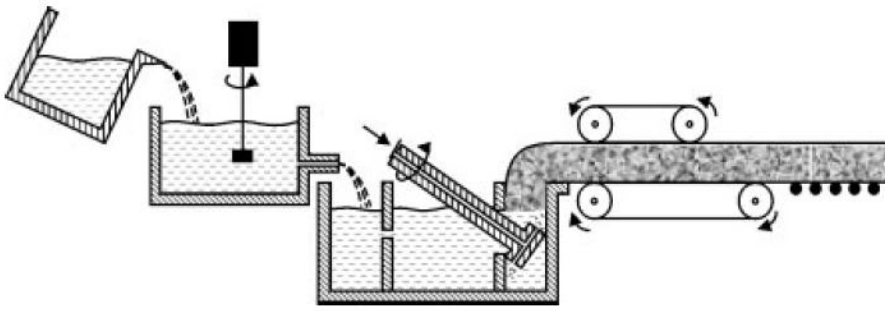

Figure 3.1. Foaming by gas injection [12].

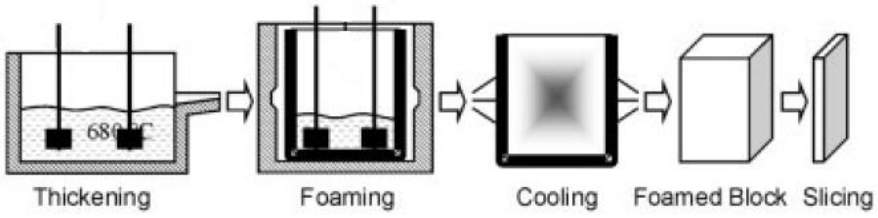

Figure 3.2. Foaming with addition of blowing agents (Alporas process) [12].

3.1.1.2 Indirect Foaming By Infiltration and Replication Processes

The replication method has been known for centuries. In this method, the replication of filler material is first formed and then the filler material is removed in order to obtain highly porous metal foam structure. The replication process can be divided into two groupes; investment casting and replication of space holder particles. Both processes involve three steps;

i) preparation of a removable pattern,
ii) infiltration of pattern with molten metal
iii) removal of the pattern

Porous metal foams with open pore structure have been produced using commercial open cell polyurethane preforms (Figure 3.3). The polymer foam with open cells is filled with slurry of refractory particles like mullite, calcium carbonate and plaster. This composite structure of polymer foam and plaster is then heat treated in order to remove the polymer preform. At a later step, the molten metal is cast into the cavities inside the mold to replicate the polymer foam structure. Casting can be done under the gravitational forces but pressure or vacuum can also be applied for filling the mold if the metal does not wet the pattern. The main difficulty in the process is the filling of the mold completely and the removal of the mold without damaging the foam structure. Generally, the refractory mold is removed by either mechanical vibration or pressurized water. This method successfully applied to manufacture aluminum [13], copper [13] and magnesium [14, 15] foams.

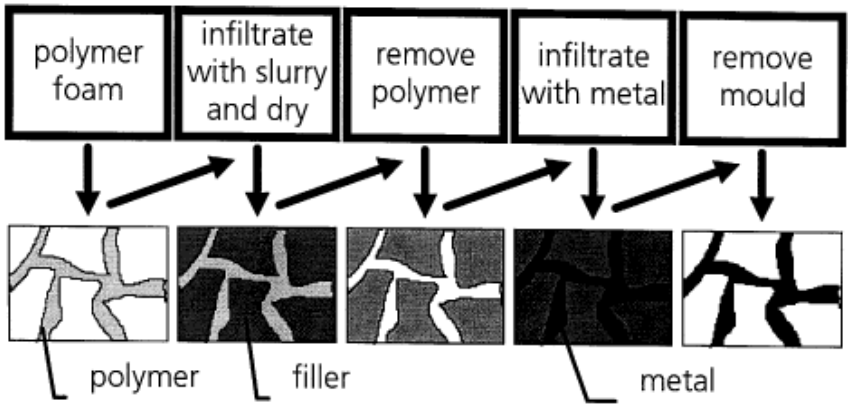

Figure 3.3. Investment casting process [16].

The alternative to the investment casting method for indirect foaming is the replication of space holder particles. This method allows the processing the foam structures with complex geometries. Basically, the process involves the casting of the melt around inorganic or organic space holder particles and then removing of the space holder particles with an appropriate method to create light weight porous metal with an open pore structure. Figure 3.4 shows the metal foam production using space holder particles. For some exceptional foams which are produced with this method, the space holder particles like hollow spheres does not removed: this kind of foams called as syntactic foam and it has closed cell structure [17]. One of the main advantages of using space holder particles is the control of the pore size and distribution which are controlled by the space holder material selection.

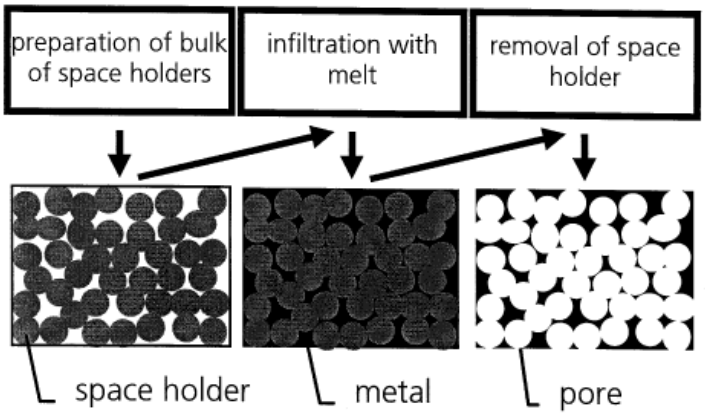

Figure 3.4. Production of metal foam using space holder particles [16].

There are several types of space holder particles, examples include inorganic soluble salts, oxide particles and organic particles. The space holder must be sufficiently refractory at the casting temperature and be chemically stable with the molten metal. There are metal foams produced by using mixture of organic polystyrene that is covered with a resin space holder material. Polymer particles are first coated with resin and then mold is filled this mixture before solidification of the resin. Resin provides the connectivity between the polymer particles. The infiltration of metal melt is done using high pressure injection machines. This method successfully applied in aluminum foam production with very short infiltration time [18]. In this very limited time polymeric particles do not have enough time for burning. After solidification, space holders are burned out in several minutes.

Inorganic space holder particles are leachable and they are removed using a solvent. The most commonly used salt space holders are NaCl [19-22] and NaF [23]. The use of NaCl salt particles as space holder has some advantages including low cost, flexibility in powder shape and size, and fast dissolution in water. Additionally, the connectivity of salt grains can be improved by sintering the salt particles. After the infiltration process, the salt particles are dissolved usually in hot water because of the higher solubility of salt particles in hot water, e.g. 100°C hot water can dissolve 39.1 g/100 ml NaCl salt. The foams can also be produced by the replication of silica bead space holders [24]. The infiltration of the molten metal is performed around the silica beads and then the space holder particles are leached with wet chemical etching method by the use of hydrofluoric acid (HF) solution. Oxide particles as in the form of both agglomerated pellets of fine grained ceramic powders or large granulated oxide particles are also used as a space holder. The removal of fine grained powder pellets can be done by spraying water on the pattern that physically breaks down the pattern into small parts or by vibration. By using pelleted silica sand, cast-iron sponges are also produced.

The indirect foaming processes have distinct advantages such as the control of the pore structure (pore size and distribution) by carefully choosing of polymeric preform or space holder particles. The main disadvantage of indirect foaming processes as compared with liquid state foaming processes is the maximum porosities that can be achieved using space holders. That are limited below 80%; however, other liquid state processes allow porosities up to 98%. On the other hand, the minimum achievable porosity level is 55% [16].

3.1.1.3. Powder Compact Melting

Metals can be foamed into the desired shapes by heating a compacted mixture of metal powder and blowing agent. This method can also be classified as powder metallurgical as the starting materials are in powder form (Figure 3.5). The foaming however takes place in the liquid state. The process starts with mixing metal powder with a blowing agent. The blowing agent is usually selected from the materials that release gases like hydrogen and carbon dioxide upon heating. Examples of blowing agents include TiH_2, ZrH_2 and calcium carbonate. After homogeneously mixing the powders, the mixture is compacted or extruded to form a dense metal powder structure.

The precursor or compacted powder mixture is then heated above the melting temperature. In the heating, the blowing agent decomposes and releases gas and forces the molten precursor to expand. The decomposition temperature of the blowing agent must be higher than the melting temperature of the metal. This process is commercialized as FORMGRIP process, to produce closed pore, near net shape aluminum foams with various shapes, e.g. plates, tubes and other complex geometries [25].

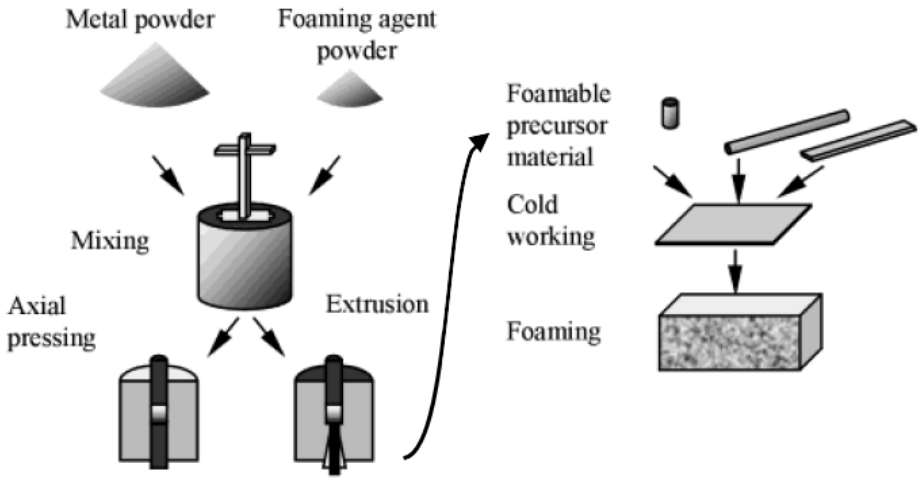

Figure 3.5. Powder compact melting process [10].

3.1.2. Solid State Processing of Cellular Metals

For some cases, it is more practical to use solid metal in powder form to make cellular metallic structures. For example, solid state processing methods are successfully applied to obtain titanium foams since the molten titanium is very reactive with the air. The powder remains in solid state during the entire process and passes through a sintering treatment or other solid state operations. In liquid state foaming, the surface tension can form closed pores, while sintering generally results in open cell structures. Solid state processing methods are also known as powder metallurgical method. Cellular metals can also be manufactured by sintering of metallic hollow spheres.

3.1.2.1. Sintering of Powder Compacts

Open cellular metals can be successfully manufactured by using powder metallurgy with space holder particles. In this method, metal powders are mixed with suitable space holder particles and then the mixture is compacted to a near net shape. The compacts are finally heat treated to i) remove the space holder particles by decomposition and ii) sinter the metal powder at relatively high temperatures to give particles uniformity. The processing steps of space holder method are shown in Figure 3.6. One of the important parameters of powder metallurgy method is the space holder selection. The size, shape, amount and distribution of the pores, which change the final properties of foam, can easily be modified by changing the space holder particles. Also the removal method depends on the type of space holder used. Ceramic particles, hollow spheres, salts, and polymer/organic grains can be used as space holders. Another important parameter is the particle sizes of powder; the metal powder must be at least three times smaller than the space holder particles [26]. Generally the organic materials and salts are selected as space holder, which can be removed thermally or dissolved by a solvent. Titanium, stainless steel and super alloy foams were prepared previously using ammonium bicarbonate, urea [26, 27], and also tapioca starch [28] as space holders. Ammonium bicarbonate and urea are removed thermally at 200°C and 450°C, respectively. Aluminum foams were prepared using raw cane sugar as space holder [29] which was removed thermally and copper foams were prepared using sodium chloride [30] space holder particles which was dissolved in water.

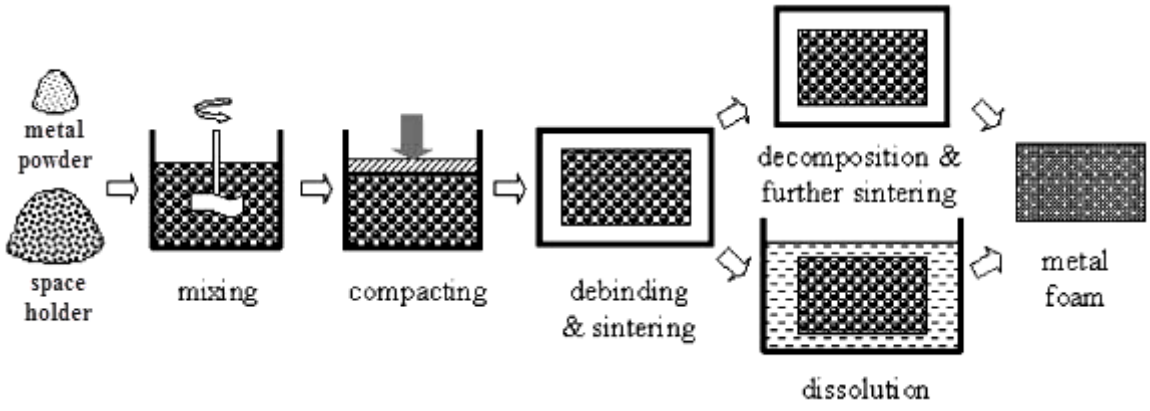

Figure 3.6. Processing steps for space holder method [26].

3.1.2.2. Metallic Hollow Sphere Process

The schematic of making cellular structures by the metallic hollow sphere process is shown in Figure 3.7. Highly porous cellular metal structures can be produced by bonding the individual spheres together through sintering. Metallic hollow spheres including copper, nickel, and titanium can be manufactured by several ways; i) decomposition of the respective metal onto polymer spheres which are removed with heat treatment or ii) coating of polymer with a metal suspension following by sintering of metal to obtain dense shell while the polymer is burned off.

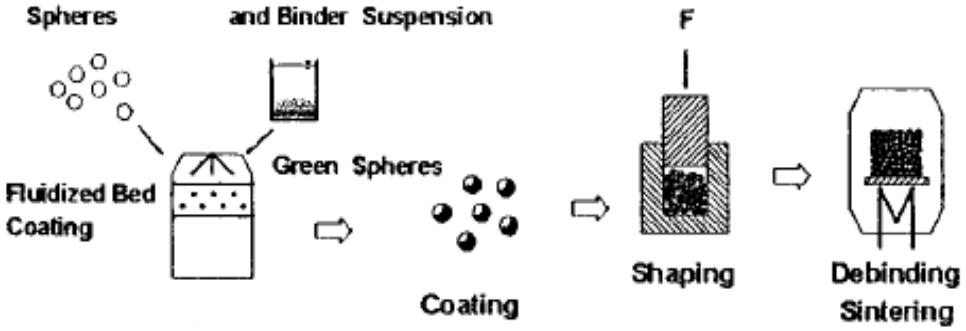

Figure 3.7. Hollow sphere process [12].

3.1.3. Deposition Methods

Decomposition of metal onto an open cell polymer foam by chemical vapor decomposition, evaporation or electrodeposition is another method for the open cell cellular metal processing. After the decomposition of metal, polymer preform is burned out by heating. This method is generally used to produce highly porous, up to 97%, cellular structures of nickel and its alloys.

Table 3.1 summarizes the production methods of cellular metals and the resultant cell topology. Decomposition method results in open cell structure as with solid state foaming processes while foams by gas injection and with blowing agent generally give close cell structure.

Table 3.1. Summary of the production methods with resulted cell topology.

	Production Method	Cell Topology
Liquid State	Foaming by gas injection	Closed pore
	Foaming with blowing agents	Closed pore
	Investment casting	Open pore
	Replication of space holder particles	Open pore
	Powder compact melting	Closed pore
Solid State	Sintering of powder compacts	Open pore
	Sintering of hollow spheres	Open pore
		Closed pore
	Deposition methods	Open pore

3.2. Manufacturing Methods for Lead Foams

In the literature research has been focused on aluminum and titanium foam processing. In the recent years, interest in lead and lead alloy foams has increased because of its potential applications in lead-acid batteries. Light weight foam electrodes could alter the drawbacks of conventional lead-acid batteries such as low specific capacities, low specific powers, short cycle life and poor charge acceptances. Alteration of these drawbacks would increase the potential of the usage of lead-acid batteries in new application areas such as electric or hybrid electric vehicles.

3.2.1. Powder Compact Melting

Lead alloy foams with densities as low as 1 g/cm^3 (Figure 3.8) were previously produced using lead carbonate as blowing agent [3]. The decomposition temperature of lead carbonate was in the range of the melting point of the used lead alloy. The metal powder and 2 wt% blowing agent was compacted through extrusion in order to create higher degree of shear in the material that broke the oxide layer around the particles and improve the bonding between particles. Foaming was performed at 450°C. The higher degree of oxygen content prevented the metallic bonding between particles and also the foaming of the compacts.

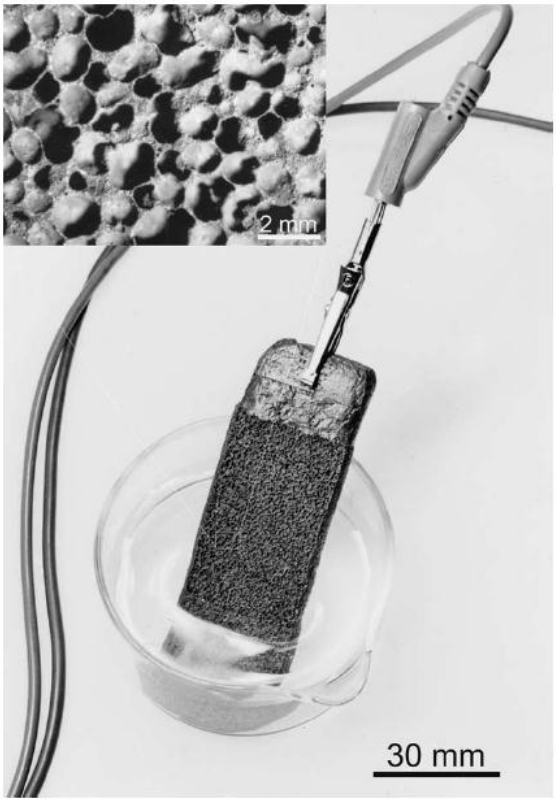

Figure 3.8. Lead foam produced by powder compact melting method [3].

3.2.2. Foaming With Liquid Metal

Another promising method for open cell lead foam processing is the replication of space filler preform by the infiltration of molten metal. Belhadj et al. [31] prepared open cell lead foams using liquid metal infiltration method. In this process, the liquid lead was penetrated into the irregularly shaped salt particles whose particle sizes varied between 1.6 to 3.15 mm. After the infiltration of the metal, salt space holder particles were dissolved in water. The mechanical properties of the prepared lead foams of 58 and 69% porous were also determined in the same study. A picture of the prepared foam is shown in Figure 3.9. The foam has open cell structure and irregular cell shapes.

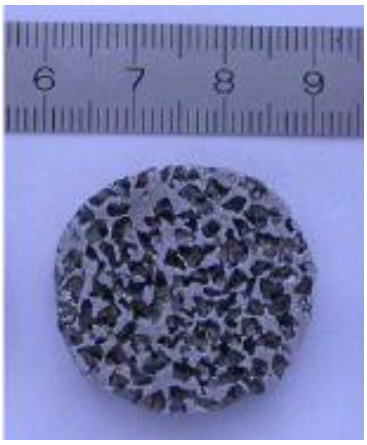

Figure 3.9. Lead foam prepared by the infiltration method, 2 mm in average pore size and 69% porous [31].

Gyenge et al. [32] prepared reticulated lead foam by casting. In the same study, the discharge performance of the prepared foams as positive electrode was also investigated. The reticulated foam structure (Figure 3.10) had a density of 2.4 g/cm^3 (79% porous, 10 pores/cm), and a specific surface area of 14 cm^2/cm^3 which was three times higher than the book-mould electrode (4.6 cm^2/cm^3). The reticulated lead collector was further shown to increase the utilization efficiency of the positive electrode by 50% during 3h discharge rate as compared with conventional grids. The use of lead foam electrode increased the discharge current density to 37.1 mA/cm^2, which was about 5 times higher than that of conventional grid electrode, 7.2 mA/cm^2.

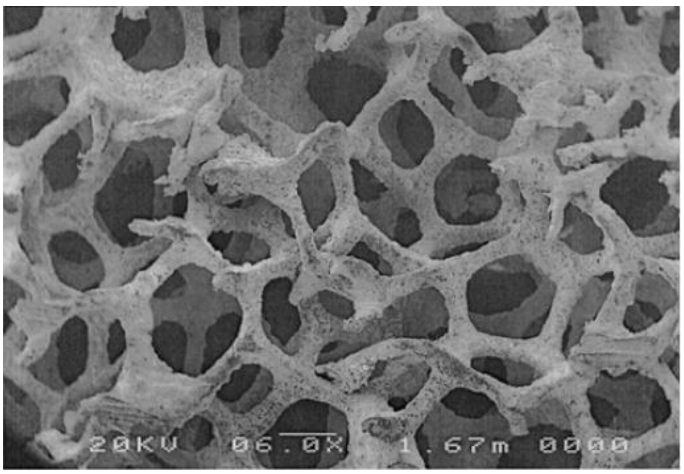

Figure 3.10. Structure of reticulated lead foam [32].

3.2.3. Deposition methods

Dai et al. [2] investigated the lead foam production by the electrodeposition of lead on a copper foam. Copper foam (20 pores per inch; surface density: 600-700 g/m^2; thickness: 2.0 mm) was used as substrate and lead was electrodeposited after the treatment of copper foam with boratofluoric acid and distilled water for few times. The measured specific surface area was about 5700 m^2/m^3 (57 cm^2/cm^3) which was 13 times higher than that of book-mould type electrode, 4.6 cm^2/cm^3 [32], offering a more effective contact between active material and electrode. Additionally, the performance of the lead foam as negative electrode in the VRLA battery (VRLAB) was investigated in the same study. It was shown that lead foam had a higher charge acceptance than the cast grid one. The higher specific surface area and contact area with the active material caused the reduction of the density of the current passing through the contact surface, the polarization resistance and the ohmic resistance of the electrode in lead foam electrode. As a result, the battery with foam electrode yielded higher discharge voltages with improved active material utilization efficiency. Besides, foam electrode provided improved fast charge performance due to both increased surface area and decreased electrochemical polarization [33].

Tabaatabaai et al. [4] prepared lead foam (Figure 3.11) with deposition method by using an organic foam compound as a substrate. The organic foam was coated with the conductive layer by the electroless method and the conductive foam was galvanostatically plated with pure lead using a fluoroborate bath. The discharge experiments of the VRLA batteries with foam electrode showed that the foam grid power density increased by 42% as compared with conventional lead grid. Figure 3.12 shows the power density difference between the batteries with foam grid and cast grid electrodes. The foam grids show lower discharge capacity reduction with increased number of cycles than the conventional cast grids.

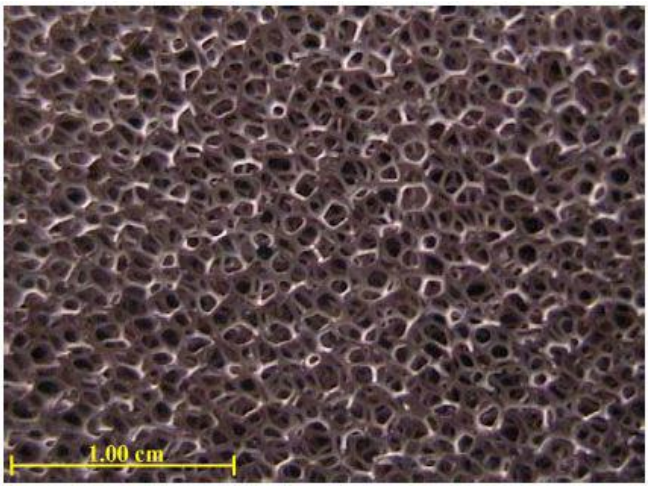

Figure 3.11. Lead foam obtained by deposition method [4].

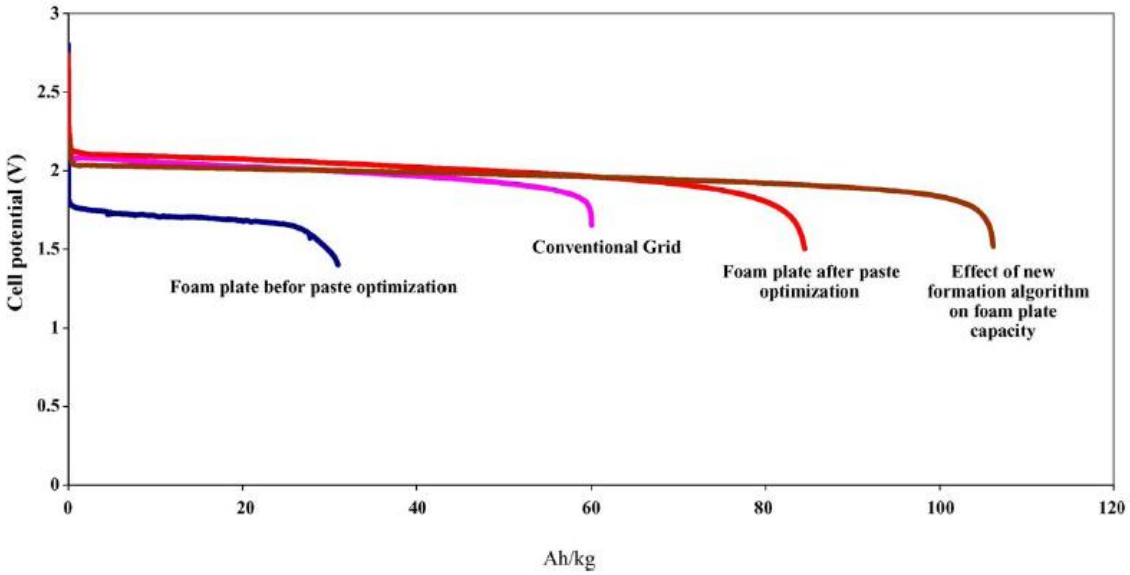

Figure 3.12. Power density of the lead foam cell compared with the conventional cell [4].

Czerwinski et al. [34] prepared lead foams by deposition method using a 20 PPI porosity reticulated vitreous carbon carrier (RVC), porous glassy carbon. RVC substrate was plated with a 15 μm thin layer of lead. It was reported that the reticulated lead structure yielded as positive active material efficiency of 56% at 4 mA/cm^2, whilst under similar conditions a typical book mould collector yielded 49% utilization efficiency.

3.3. Characterization of Cellular Metals

The density of a cellular material can be determined by weighing it and by measuring its volume using Archimedes' principle. According to this principle, liquid should not be penetrated into pores of metal. If the sample to be characterized does not have a dense outer skin, penetration of liquid into the pores has to be prevented by coating the surface with a polymer or paraffin film. The second method is basically measuring the mass and calculating the volume of the simple shape foam sample and determining the ratio of mass to volume.

The liquid processing methods yield cellular materials with close cells with a dense outer skin. However, in practice imperfections can form while making the foams. Such imperfections include small size voids or cracks in the cell walls or on the outer skin. Penetration techniques are ideal for detecting such surface defects.

3.3.1. Optical Image Analysis

The cell morphology and microstructure of cellular metals can be analyzed by microscopic techniques. Although the actual analysis is nondestructive, sample preparation usually requires cutting, embedding and polishing and is therefore becoming a destructive technique. Optical image analysis programs help to investigate the structure of cellular materials from images taken by optical or electron microscopes. With the help of the optical image analysis methods the pore size and distribution can be determined. In order to obtain representative results, foam materials should be prepared very carefully. For optical image analysis, cellular metal is embedded in a resin and then polished. The reason for the resin embedding is creating contrast between the pore walls and the interior of the pores. Also embedding prevents the deformation of the cells during sample preparation.

3.3.2. Mechanical Testing

The resulting mechanical properties of the foam samples with same density may show a larger scatter than those of conventional materials. In order to obtain meaningful

results a high number of samples may be required as compared with non-cellular materials. Also, as in cellular materials the length scale for macroscopic heterogeneities is sometimes in the range of millimeters, the sample dimensions in mechanical tests are larger than conventional test sample size. For the testing of the cellular metals, "DIN 50134 standard: testing of metallic materials – compression test of metallic cellular materials" was developed in order to standardize the mechanical testing of cellular metals [35].

The loading rate can be constant, slowly increasing, dynamic or cyclic. In literature, most of the works are carried out under quasi-static strain rates, 10^{-2} or 10^{-3} s^{-1}. High strain rates can also be applied using drop weight test (up to 100 s^{-1}), and Split Hopkinson Pressure Bar Test (up to 5.10^{3} s^{-1}). Fatigue tests are most easily carried out in a compression–compression mode for the same reasons which apply to quasi-static tests, but compression–tension, tension–tension and cyclic bending tests have also been performed by preparing and fixing appropriate samples. Creep tests are carried out under given constant loads. Other mechanical tests include fracture toughness measurements on notched samples and hardness tests with various indentor shapes.

CHAPTER 4

PROCESSING METHODS

4.1. Lost Carbonate Sintering Method

The specifications of lead and ammonium bicarbonate powders used to prepare sintered lead powder compacts are tabulated in Table 4.1. The particle size of the lead powder determined using a Malvern Mastersizer 2000 particle size analyzer is shown in Figure 4.1. The particle size ranges between 20 μm (d_{10}) and 96 μm (d_{90}) with an average size of 48 μm (d_{50}). As-received lead powder has irregular shape particles as shown in Figure 4.2(a). Initially, ammonium bicarbonate particles were sieved (ISO 3310-1) in order to obtain narrower particle size distribution, in the range of 315-500 μm (Figure 4.2(b)). This particle size range satisfies the requirement that the particle size of the space holder must be bigger than the metal powder particle size for a good packing between powders. The decomposition of ammonium bicarbonate [36] proceeds with the following reaction;

$$NH_4HCO_3 \rightarrow NH_3 + H_2O + CO_2 \quad (4.1)$$

The decomposition temperature of ammonium bicarbonate was determined previously and shown in Figure 4.3. The decomposition as shown in the same figure starts at about 50 and ends up at 185°C (Figure 4.3).

Table 4.1. Raw material specifications

Powder	Company	Particle Size	Purity
Lead Powder	Alfa Aesar	-200 mesh (d_{50}: 48 μm)	99%
Ammonium Bicarbonate	Merck	-500, +314 μm	98%

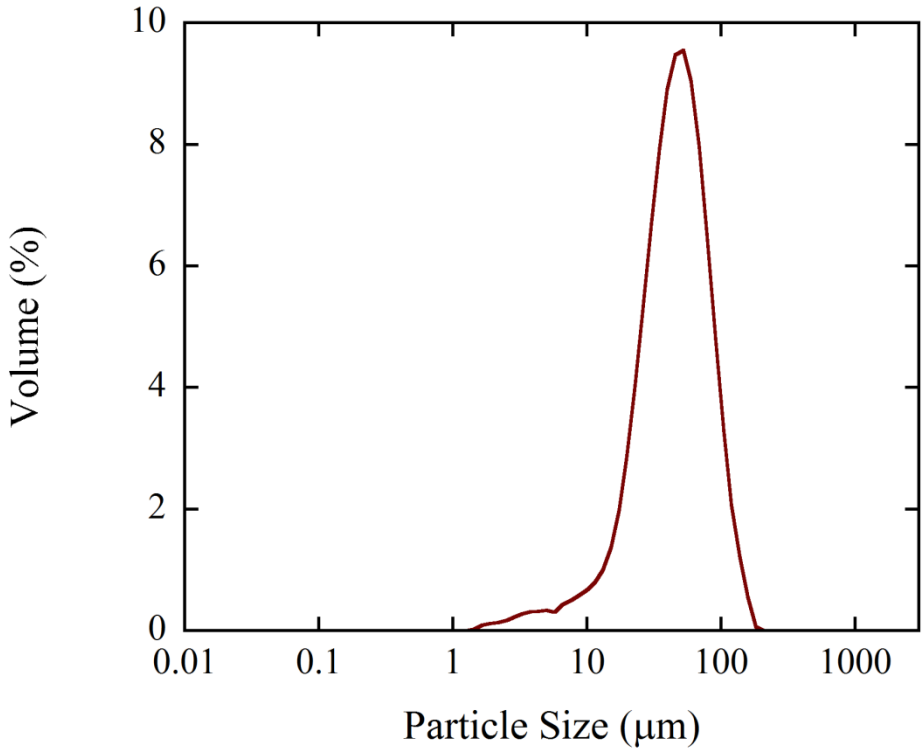

Figure 4.1. Particle size distribution of lead powder.

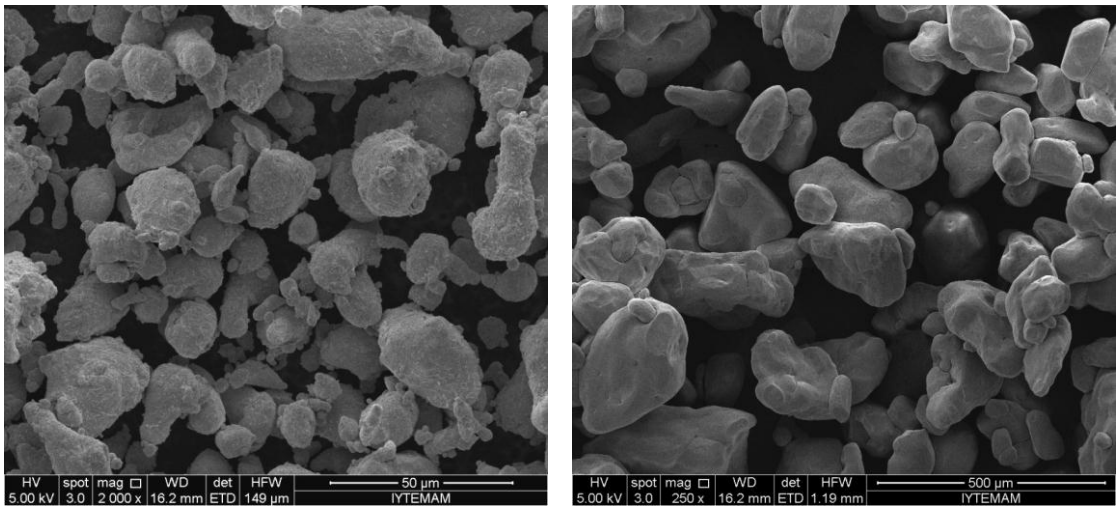

(a) (b)

Figure 4.2. SEM micrographs of as-received (a) lead powder particles and (b) ammonium bicarbonate particles.

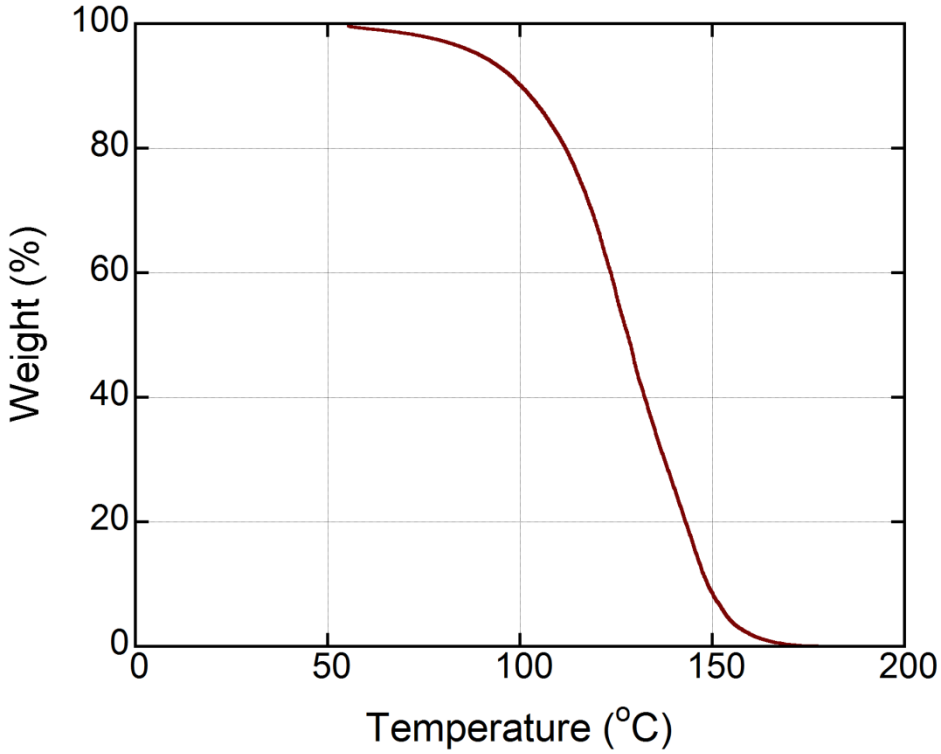

Figure 4.3. TGA curve of ammonium bicarbonate [37].

The applied foam preparation method is schematically shown in Figure 4.4. The foaming process starts with the mixing of lead powder with 50 volume% ammonium bicarbonate space holder to give a 50% porous foam structure. The weights of lead and space holder were calculated using the following relations

$$Weight_{Pb} = \frac{Volume_{foam}(100 - \%Porosity) * \rho_{Pb}}{100} \quad (4.2)$$

$$Weight_{ABC} = \frac{Volume_{foam}(100 - \%Porosity) * \rho_{ABC}}{100} \quad (4.3)$$

where ρ is the density and ABC refers to ammonium bicarbonate. In the calculations the density of lead and ammonium bicarbonate were taken sequentially as 11.34 and 1.59 g/cm^3. Since the used lead alloy is a relatively soft material and provides lubrications between particles no binder was used in the powder mixing and compaction. The powder mixing was carried out in a plastic container by means of a spoon. Green powder compacts with a diameter of 25 mm and a thickness about 11 mm were then cold compacted at room temperature inside a stainless steel die (Figure 4.4). The

compaction was performed under 71, 142 and 204 MPa pressures using a Schimadzu AG-IX universal tension-compression at cross-head speed of 0.5 mm s^{-1}. Green compacts were then heat treated at 200°C for 2 h in a Labart Vacuum Furnace at 0.986 atm pressure to minimize the further oxidation of the lead powders during ammonium bicarbonate decomposition. The resulting porous lead green powder compacts were finally sintered in a tightly closed horizontal tube furnace under high purity (99.998%) Ar flux (6 cm^3 min^{-1}) at temperatures ranging between 261°C (0.8 T_m) and 300°C (0.9 T_m) for 2 h. The heating profile of the tube furnace sintering at 261°C is shown in Figure 4.5. The heating of the compact from room temperature to sintering temperature takes about 0.5 h. Quasi-static compression tests samples, 8 mm in diameter and 11 mm in height were prepared through core drilling. During core drilling, applied pressure was kept as small as possible in order to eliminate any deformation of the foam sample.

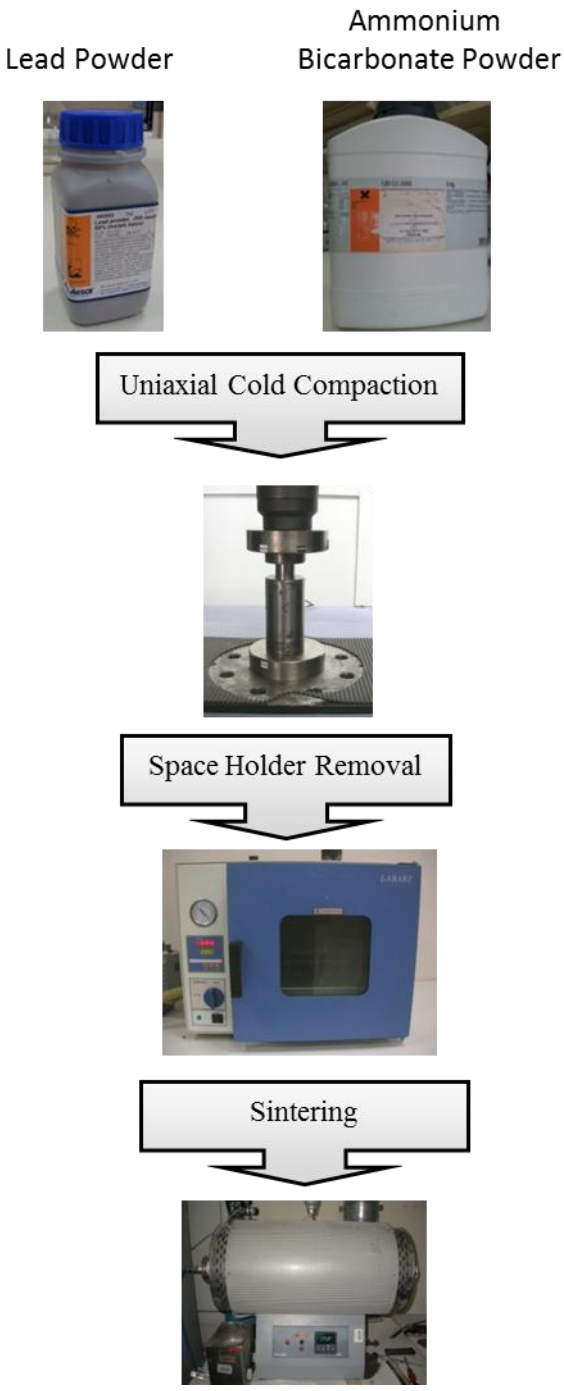

Figure 4.4. Foaming process for powder metallurgy method.

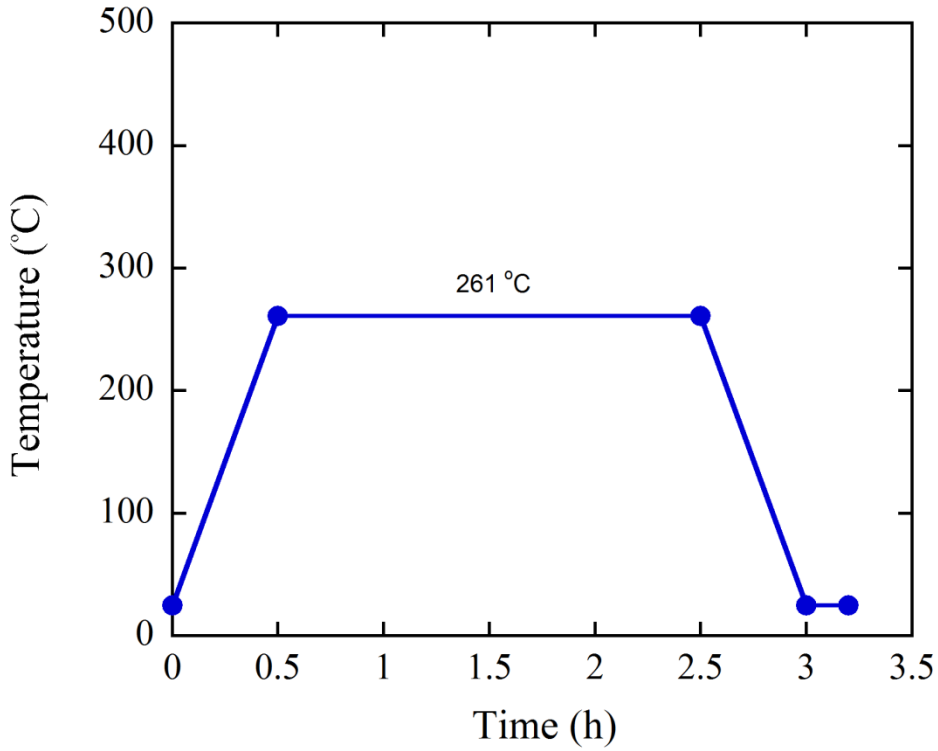

Figure 4.5. Heating profile of tube furnace during sintering process.

The density of foams was determined by dividing the weight of the samples to the volume of samples. The percent porosity (P) was calculated using the following relation

$$P = (1 - \frac{\rho_{foam}}{\rho_{Pb}}) * 100 \quad (4.4)$$

where ρ_{foam} and ρ_{Pb} are the density of the foam and bulk lead, respectively.

4.2. Electro-winning Method

Foam lead processing was tried through electro-winning of a secondary phase in the matrix phase. This method is generally used for electro-deposition of metals from their ores in an electrolyte solution by applying electrical current to the anode and cathode electrodes. Basically, the method consists of melting of secondary and matrix phase elements together and solidification prior to the removal of the secondary phase through electro-winning. Lead was chosen as a matrix metal with a secondary phase

selected from immiscible elements. Zinc and copper are two elements forming immiscible phase in lead as sequentially shown in the phase diagrams in Figure 4.6 and 4.7.

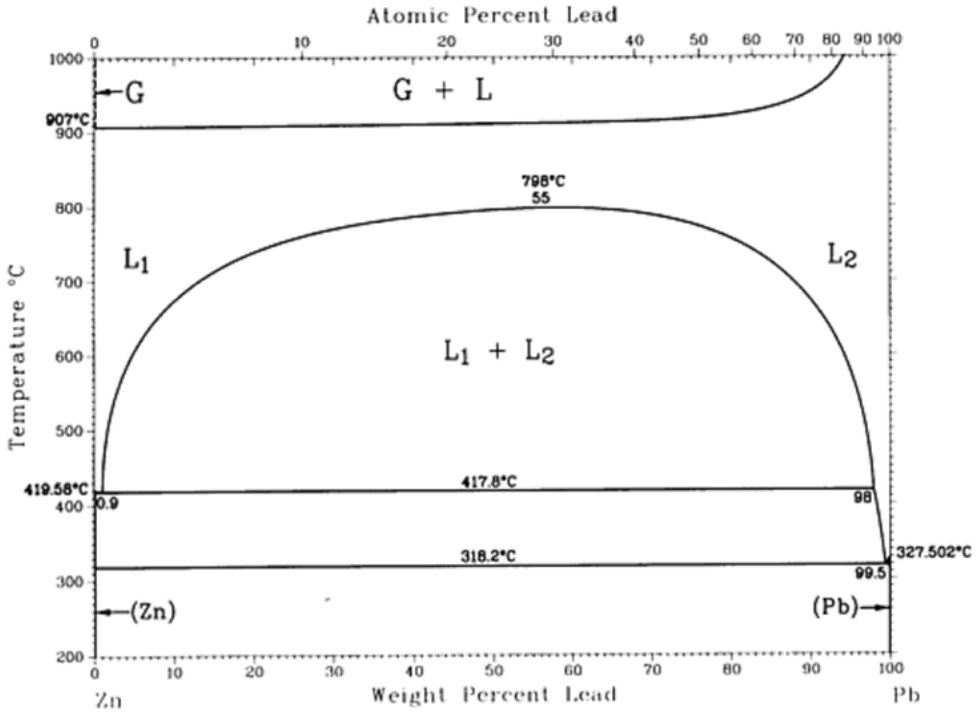

Figure 4.6. Binary phase diagram of Zn-Pb [38].

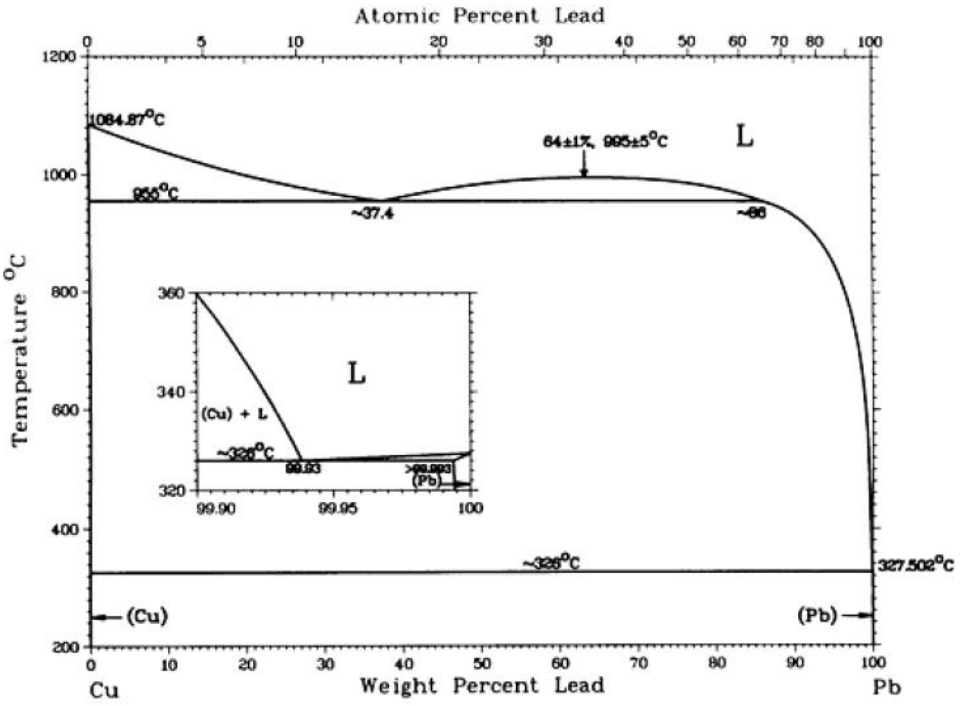

Figure 4.7. Binary phase diagram of Cu-Pb [38].

The stages of preparation of samples for electro-winning are shown in Figure 4.8. Lead was melted with 50 volume% of zinc or copper to obtain 50 volume% secondary phases within lead matrix. Lead and zinc form immiscible liquid phases above 417°C (Figure 4.6) and lead and copper above 995°C (Figure 4.7). Zinc-lead system was melted at 600°C and copper-lead system was melted at 1200°C. Both melting processes were done in silicon carbide crucibles inside a preheated box furnace. After melting of metals, crucible was shaken to mix the molten metals and the molten alloy casted into a cylindrical steel die. Steel die was not preheated in order to provide fast cooling of the metals. Electrowinning experiments were carried out with the thin slices (1 mm) of samples which were cut with high precision diamond saw from casted alloys. The experimental set-up used in the electrowinning process is shown in Figure 4.9. Electrowinning samples were used as anode metal and 316L stainless steel plate with 50 mm width and 100 mm length was used as cathode material. The electrolyte consisted of sulfuric acid (H_2SO_4), and deionized water. Starting electrolyte was freshly prepared before each experiment by using sulfuric acid (Panreac - 97%) with 180 g/l concentration and pure water [39]. Before each experiment, stainless steel cathode was wet sanded with 600 grit silicon carbide sandpaper, washed with pure water and air dried to clean of the surface and also during the experiments to obtain highest amount of copper that was collected on the cathode; cathode was cleaned every hour of electrowinning. Experiments were carried out in a glass container that contained electrolyte and electrodes. The electrodes were separated at a distance of 20 mm. Direct current was supplied using a GNC-HY1803D power supply (0-18 V and 0-3 A). The maximum current efficiency was previously determined at 300 A m^{-2} current density [39]; therefore the current determined 1.4 A for the studied electrowinning cell. During experiments the electrolyte temperature was kept constant at 60°C and the electrolyte was continuously mixed on a Stuart CB162 hot plate. Microstructure analysis of the samples after and before electrowinning experiments were carried out in SEM and the polished cross-section of the microscopic samples was etched with a solution of 10 ml H_2O and 50 ml HNO_3 [40].

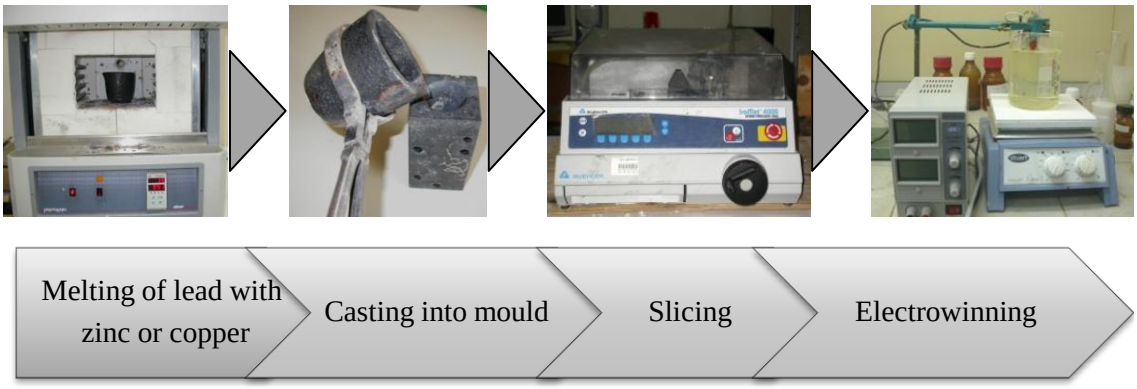

Figure 4.8. Experimental process of electro-winning method.

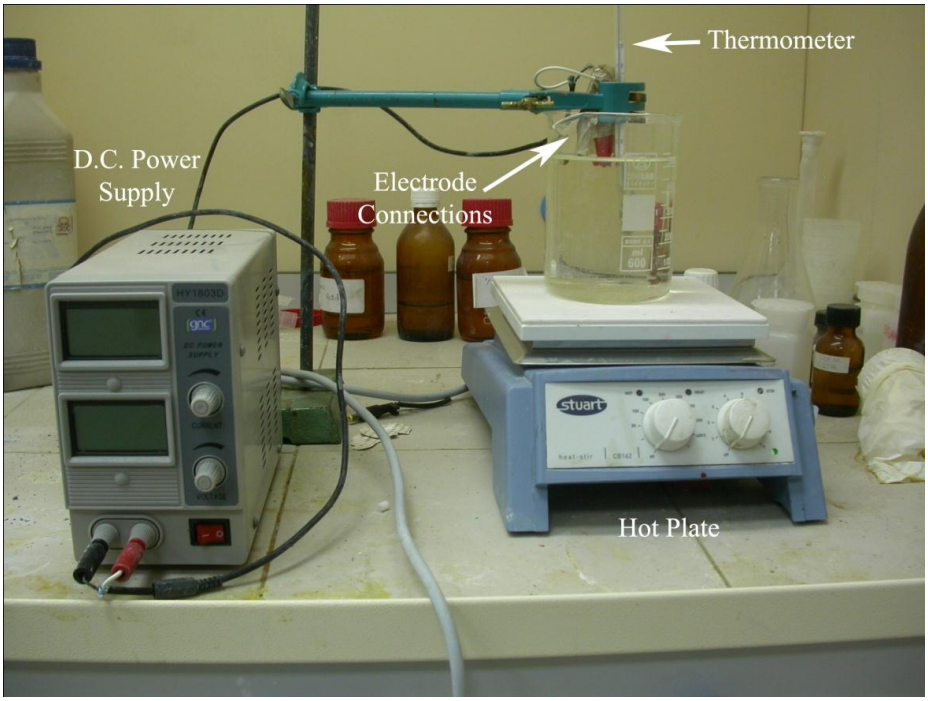

Figure 4.9. Experimental setup for electrowinning.

4.3. Replication of Space Holder Particles

The chemical composition of the alloy used in this method was determined using a METEC-Spectro IQ-II XRF and is tabulated in Table 4.2. Two different space holding fillers were used to prepare lead foams: silica beads (Sigma S7500 Type-II and Performans-131335) with particle sizes of 2 and 2.5 mm (Figure 4.10(a)) and salt powder (Figure 4.10(b)) with an average particle size of 440 µm (max: 591 µm, min: 380 µm). The average particle size was measured from SEM images using an Olympus Scandium software.

Table 4.2. Chemical composition of lead alloy.

Element	Pb	Ca	Sn	Al	Ag	As	Bi	Cu	Fe	Ni	Te	Zn	Sb	Cd
Weight%	64.85	7.5	25	0.8	0.2	0.1	1	0.1	0.1	0.05	0.05	0.1	0.1	0.05

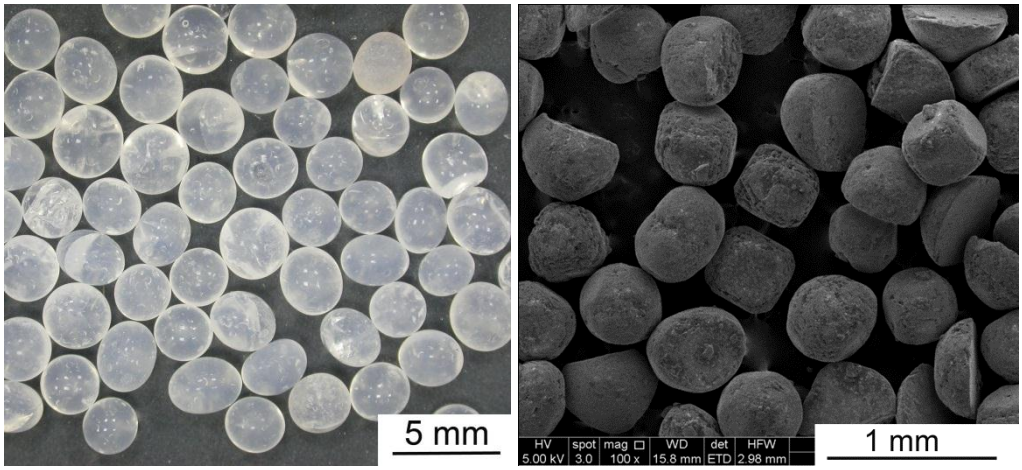

(a) (b)

Figure 4.10. (a)Optical microscope picture of silica beads and (b) SEM image of salt particles.

Before infiltration, silica beads were heat treated at 650°C for 2 h and salt particles were heat treated at 90°C for 10 h in vacuum furnace. The weight of space holder was calculated using the following relation,

$$Weight\ of\ spce\ holder = \frac{Volume_{foam}(100 - \%Porosity) * \rho_{space\ holder}}{100} \qquad (4.5)$$

where $\rho_{space\ holder}$ is the density of space holder (silica beads 0.7 g/cm^3 and salt 2.165 g/cm^3). The schematic of the foam preparation shown in Figure 4.11 and was composed of melting, infiltration and dissolution steps. The process started with the insertion of silica beads into a steel mold (Figure 4.12) and the mold was heated to the 425°C in a tube furnace as shown in Figure 4.13 .Bulk lead alloy was added into the mold after waiting 45 minutes in order to reach of the mold temperature to 425°C. After the melting of the lead, infiltration piston was moved slowly and forced the metal for the infiltration around space holder particles. The pressure for the infiltration was provided using Schimadzu AG-I universal tension-compression test machine (Figure 4.15). After

solidification of lead alloy, the space holder silica beads were dissolved inside 75% hydrofluoric acid (HF) solution for 2 h. The reaction between silica beads and HF is [41]

$$SiO_2 + 4HF \rightarrow SiF_4 + 2H_2O \quad (4.6)$$

After the completely removal of the silica beads, samples were cleaned with pure water.

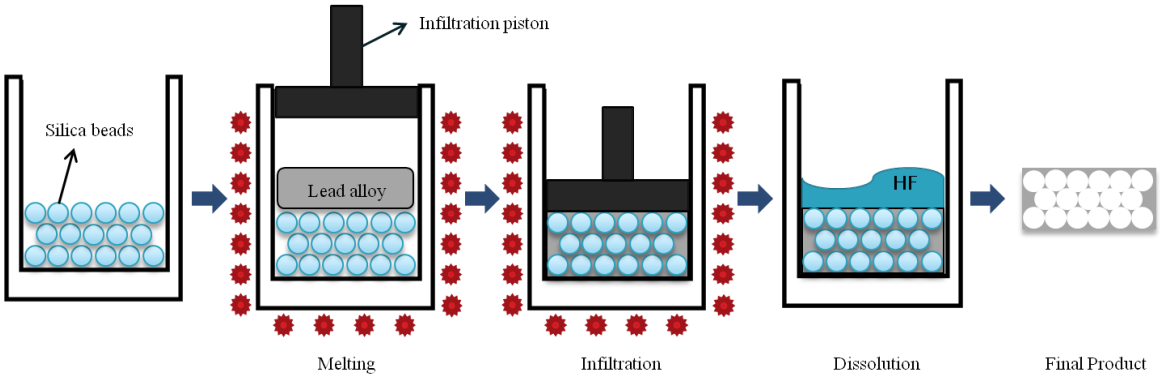

Figure 4.11. Schematic of the casting liquid metal around space holding fillers method.

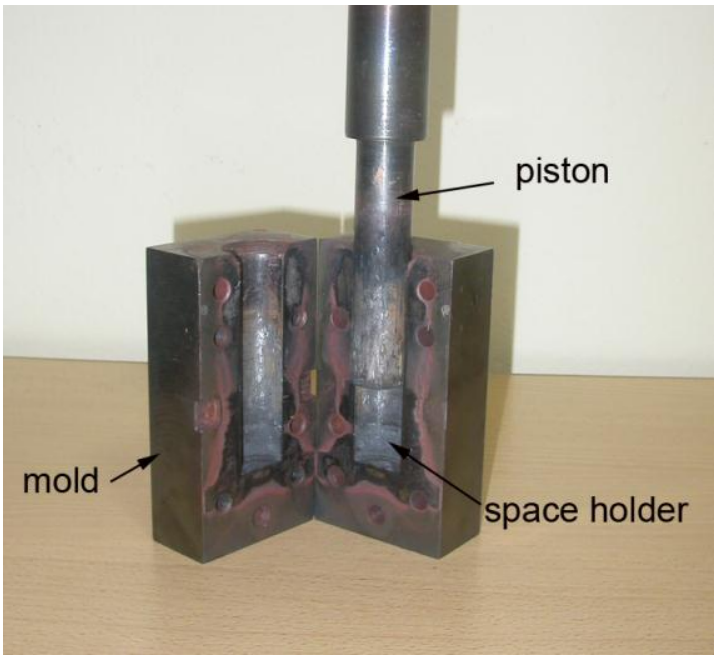

Figure 4.12. Specially designed infiltration mould.

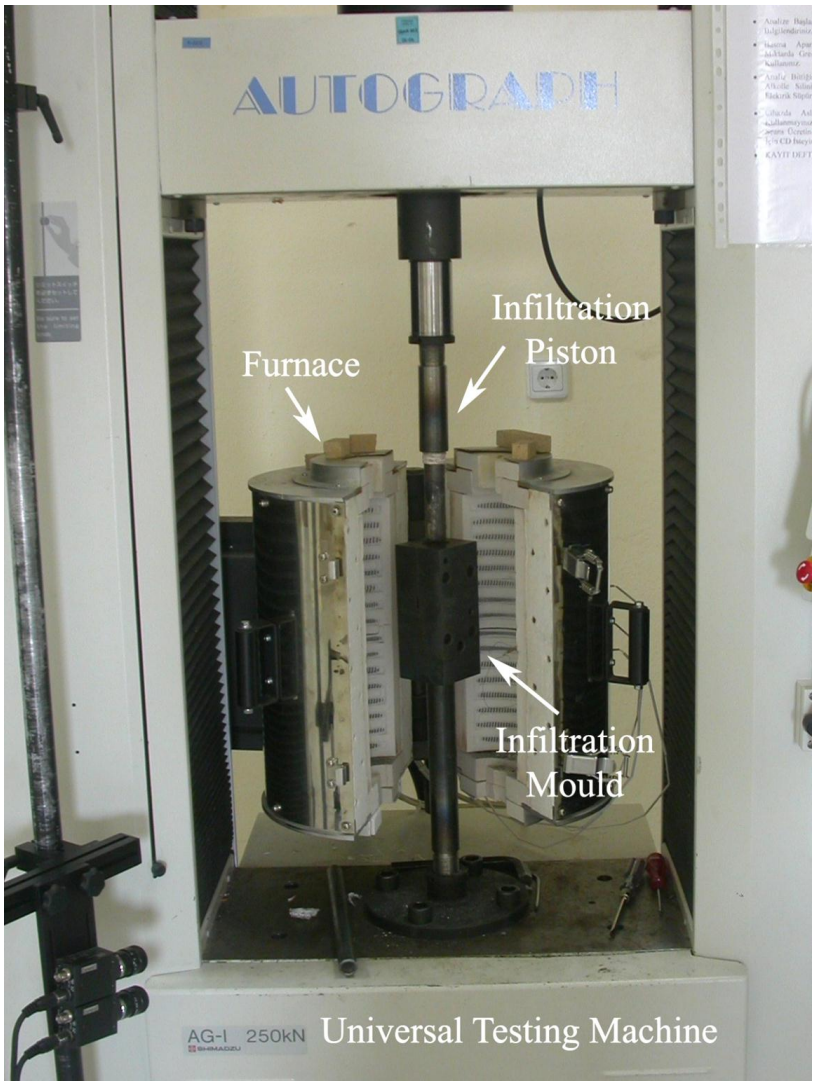

Figure 4.13. Experimental setup for infiltration process.

The applied infiltration process for salt was the same with the silica beads; the salt particles were inserted into the infiltration mold and the mold was heated up to 450°C; then, the liquid lead was infiltrated using the piston. After solidification, salt particles were dissolved in boiling deionized water under vacuum for 2 h and the process was repeated for several times. The solubility of NaCl in water is as high as 39.1g/100ml at 100°C [42]. The applied vacuum allowed water penetration through narrow interconnection regions between pores and provided complete dissolution of salt particles. After space holder removal process foam samples were dried in a vacuum oven for 5 hours at 90°C. The compression test samples of cast foams were 25 mm in diameter and 15 mm in thickness.

Compression tests on foam samples were conducted at a cross-head speed of 10^{-2} mm s^{-1} corresponding to a strain rate of $1x10^{-3}$ s^{-1}, by following DIN 50134 standard:

testing of metallic materials-compression test of metallic cellular material [35]. During the compression test, surfaces of the cross-heads were lubricated in order to reduce the frictional forces that occur between sample and compression plates. Microscopic analysis was performed on lead foam samples and samples vacuum epoxy mounted using a Meiji Optical Microscope and FEI Quanta250 FEG Scanning Electron Microscope (SEM).

CHAPTER 5

RESULTS

5.1. Powder Metallurgy Route

5.1.1. Thermogravimetry Analysis of Space Holder Particles

Thermogravimetric analysis (TGA) results of ammonium bicarbonate and urea are shown in Figures 5.1(a) and (b), respectively. Ammonium bicarbonate completely decomposes at about 150°C, while urea decomposition takes place gradually in 2 steps; the weight lost is 61% until about 250°C and the decomposition is completed at about 450°C.

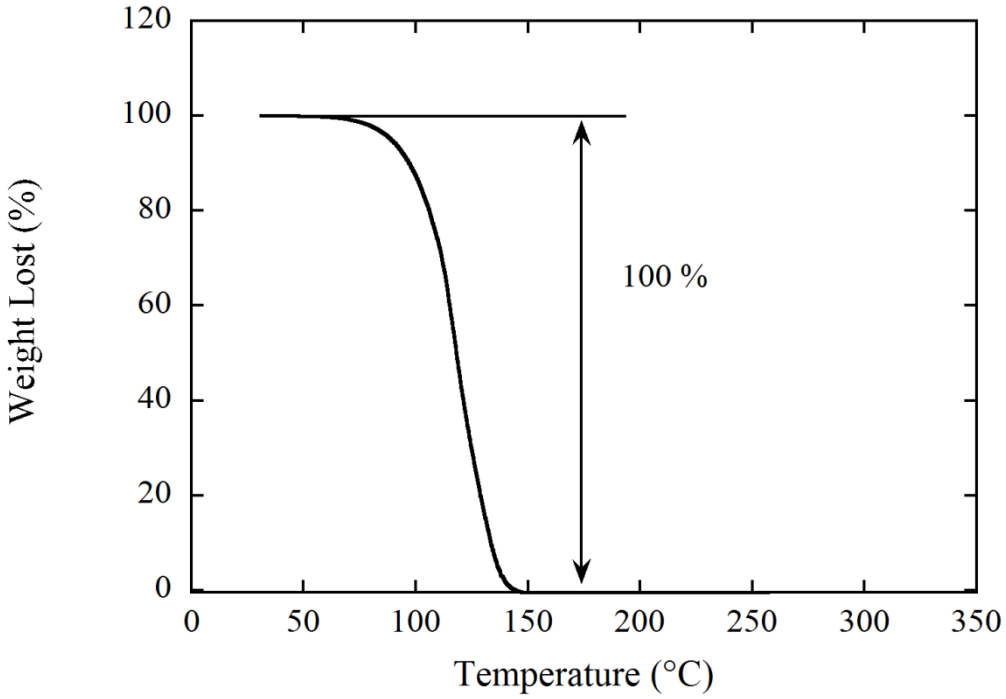

(a)

Figure 5.1. TGA curves of (a) ammonium bicarbonate and (b) urea.

(cont. on next page)

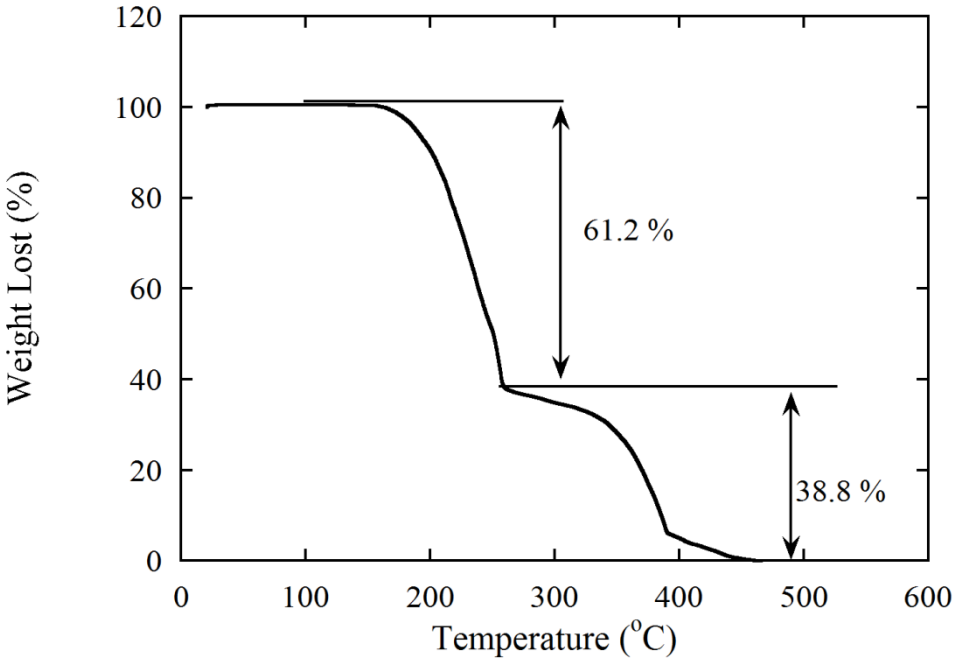

(b)

Figure 5.1. (cont.)

5.1.2. Porosity

The porosities of the foams prepared by powder metallurgical route are tabulated in Table 5.1, together with the applied compaction pressures, space holder ratio, sintering temperatures, sintering times and green compact porosities. T1 and T2 samples are the samples that are directly compression tested without sintering after space holder removal. The porosities of the sintered foams vary between 51 and 48%. The final density is solely a function of applied compaction pressure: the green compact density increases with increasing compaction pressure, while sintering at different temperatures has no significant effect on the final porosities of the green compacts.

Table 5.1. The process parameters and porosities of the foams prepared by powder metallurgy.

Sample	Compaction pressure (MPa)	Ammonium Bicarbonate ratio (vol%)	Sintering temperature (°C)	Sintering time (h)	Green compact porosity (%)	Sintered sample porosity (%)
T1	71	50	-	-	51.4	-
T2	142	50	-	-	48.4	-
T3	71	50	261	2	51.3	51.0
T4	142	50	261	2	48.3	48.1
T5	142	50	286	2	48.5	48.1
T6	142	50	300	2	48.4	48.0

5.1.3. Compression Mechanical Properties

The compression stress-strain curves of the foams prepared by powder metallurgy are shown in Figure 5.2. The prepared foams exhibit elastic-brittle compression deformation behavior. Following the linear elastic region and the associated maximum or peak compression stress, the samples fail catastrophically which is reflected as sudden reductions in stress values in the stress-strain curves. Following the initial elastic region, the stress values decrease until about complete crushing. The complete crushing followed by the compression of the failed samples causes the stress values to increase at increasing strains above 0.5. The collapse stress or maximum compressive stresses determined from the initial region of the stress-strain curves and the corresponding strain values which are taken as the failure strains are further tabulated in Table 5.2. The collapse stresses range between 2.62 and 9 MPa and the failure strains between 0.019 and 0.033.

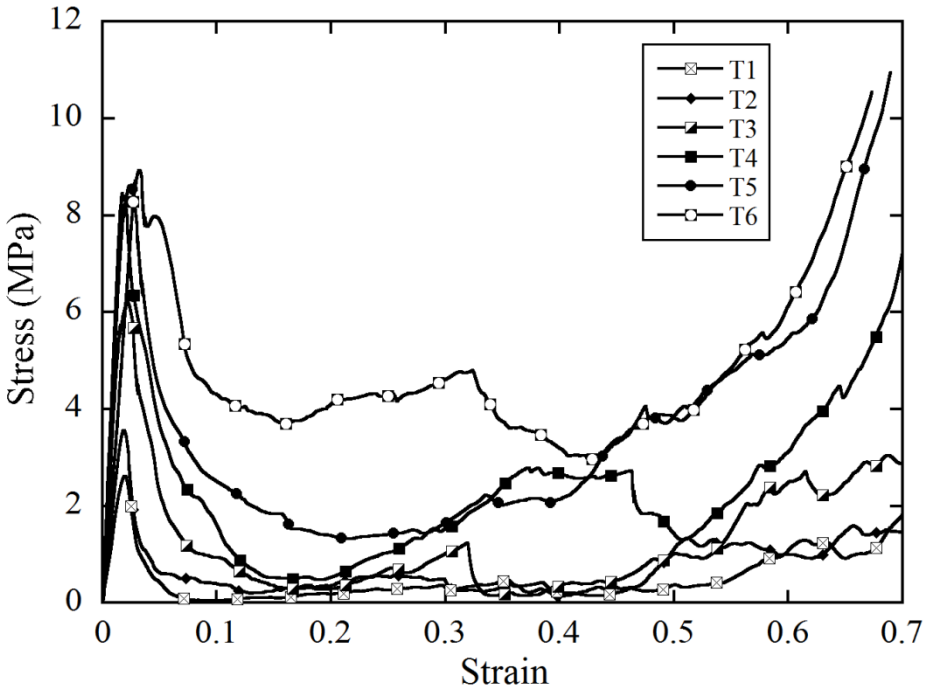

Figure 5.2. Compression stress-strain curve of the foams prepared by powder metallurgy.

Table 5.2. Collapse stress and failure strains of the foam prepared by powder metallurgy.

Sample	Collapse Stress (MPa)	Failure Strain
T1	2.62	0.019
T2	3.54	0.017
T3	6.20	0.021
T4	8.41	0.018
T5	8.57	0.023
T6	9.00	0.033

Comparisons between T1 and T3 and T2 and T4 samples clarify the effect of sintering on the collapse stress and failure strain of the foams. T1 and T3 and T2 and T4 foam samples are prepared using the same processing parameters except T1 and T2 foam samples are not passed through sintering stage; that is they are directly compression tested. As tabulated in Table 5.2, T4 and T3 samples have higher collapse stresses and failure strains than T1 and T2 samples. The collapse stress increases from 2.62 MPa in T1 to 6.20 MPa in T3. Similarly, the collapse stress increases from 3.54 MPa in T2 to 8.41 MPa in T4. The increases in stress values are only seen in the elastic regions, in the following crushing regions, the stress values of both sintered and unsintered samples approach each other.

Comparisons between the collapse stress and failure strains of T1 and T2 and T3 and T4 show the effect of compaction pressure on the compression behavior. Increasing compaction pressure increases the collapse stress values, while it slightly decreases the corresponding failure strain values as tabulated in Table 5.2. Collapse stress increases from 2.62 to 6.2 MPa and from 3.54 to 8.41 MPa for the foams compacted at 71 MPa and 142 MPa, respectively.

As the sintering temperature increases the collapse stress increases slightly. T4, T5 and T6 foams are processed with the same process parameters (142 MPa compaction pressure and 2 h of sintering time) but sintered at 261, 286 and 300°C, respectively. As the sintering temperature increases from 261°C to 286°C, the collapse stress increases only about 0.16 MPa. The collapse stress increases from 8.41 to 9.0 MPa as the sintering temperature increases from 261°C to 300°C. The failure strain increases from 0.018 to 0.033, as the sintering temperature increases from 261°C to 300°C.

5.1.4. Microscopy

The pore structure SEM images of the foam samples compacted at 71, 142 and 204 MPa are shown in Figures 5(a-c), respectively. The pore shapes seen in the same figures are angular, which is dictated by the starting shape of the space holder. The pore sizes of the foams are measured through SEM micrographs and tabulated in Table 5.3. The compaction pressure is found to be very effective in decreasing average pore sizes of the foams. As the compaction pressure increases from 71 MPa to 204 MPa, the average pore size decreases from 231 to 121 μm.

The picture of the polished surface of a foam sample prepared by powder metallurgical route is shown in Figure 5.4. Two distinct regions in the microstructure are seen; white and gray regions. The gray region around the particles is marked with an arrow in the inset of the same figure. The EDX analysis results, as tabulated in Table 5.4, indicate that white regions are high in lead content, while the gray regions are rich in oxygen. The small black particles seen in the SEM micrograph in the inset of Figure 5.4 are the SiC particles, which are the remnant of the polishing solution. The SEM image of the typical fracture surface of lead foam prepared by powder metallurgical route is shown in Figure 5.5. The cracks (marked with arrow) around the particles (intergranular) indicate the brittle nature of the foams.

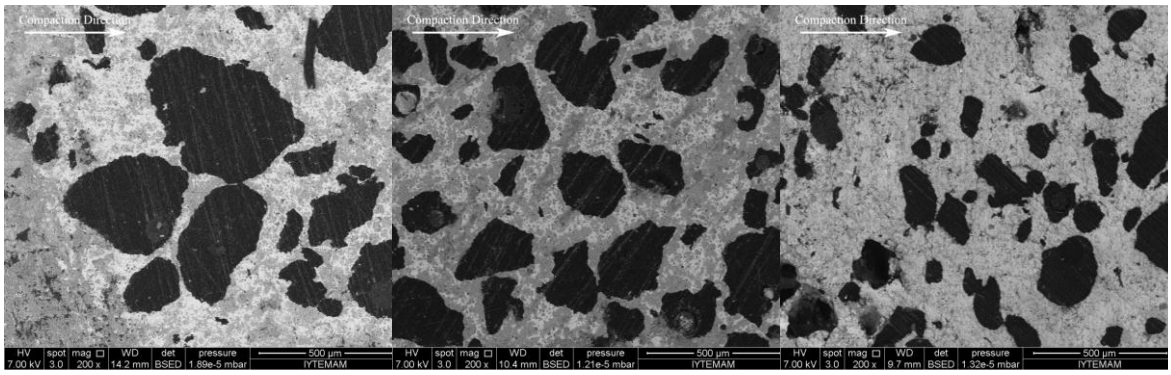

(a) (b) (c)

Figure 5.3. The pore structure SEM images of the foam samples compacted at (a) 71.MPa, (b) 142 MPa and (c) 204 MPa

Table 5.3. The average pore size of the foams prepared by powder metallurgy.

Compaction Pressure (MPa)	Average Pore size (µm)
71	231
142	181
204	121

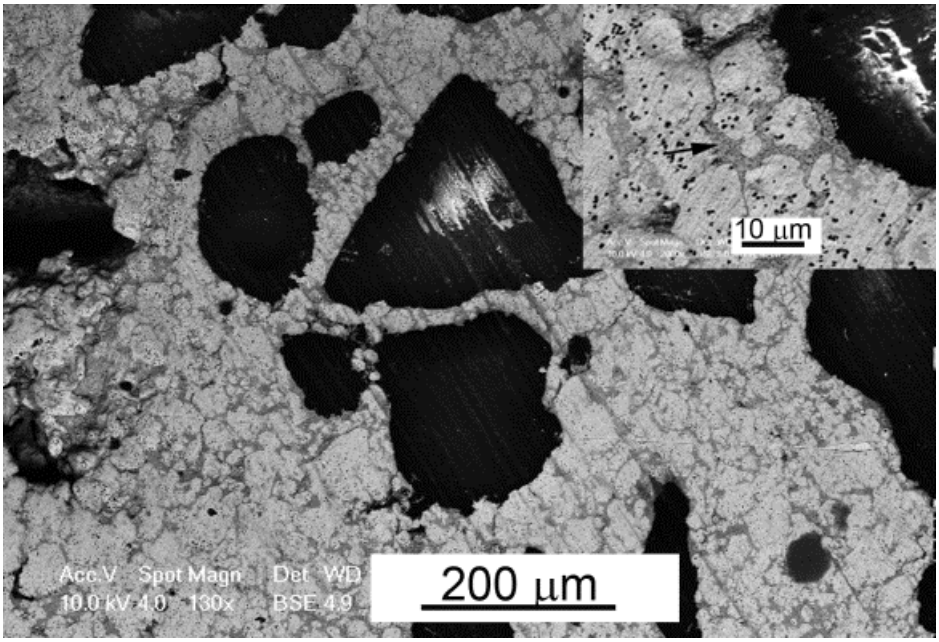

Figure 5.4. Microstructure of the polished surface of the foam.

Table 5.4. EDX results of polished surface of foams prepared by powder metallurgy.

Region	Elements (wt%)		
	Pb	O	C
White	89	6	5
Gray	72	12	15

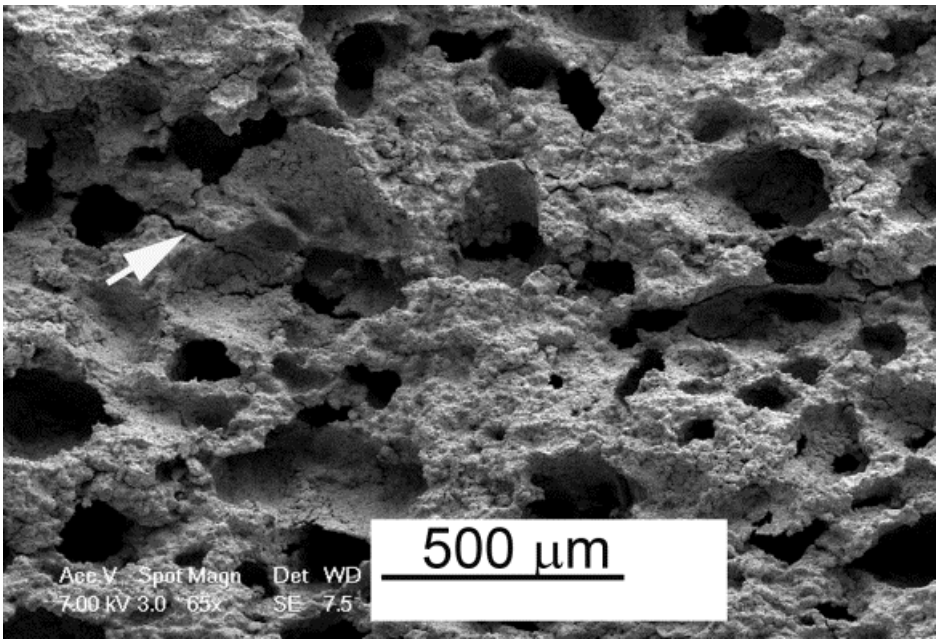

Figure 5.5. Typical fracture surface of the foam sample prepared by powder metallurgy.

5.2. Electrowinning Method

5.2.1. Zinc-Lead and Copper-Lead Binary Systems

The cross-section image of the polished surface of 50 volume% zinc-lead cast structure is shown in Figure 5.6. Two different sections are seen in the cast structure arising from density difference between lead and zinc. The upper section is zinc and the bottom section is lead. Zinc metal having a relatively lower density (6.6 g/cm^3) is solidified over the higher density lead (11.34 g/cm^3).

The SEM micrographs showing the microstructure of 50 volume% copper-lead binary cast system are shown in Figures 5.7 (a) and (b). The copper (dark regions) is seen to be distributed in lead matrix in the form of small lamellar or droplets. The sizes of copper phase vary between 8 and 48 µm (see Figure 5.8 for the measurements) with an average size of 18 µm.

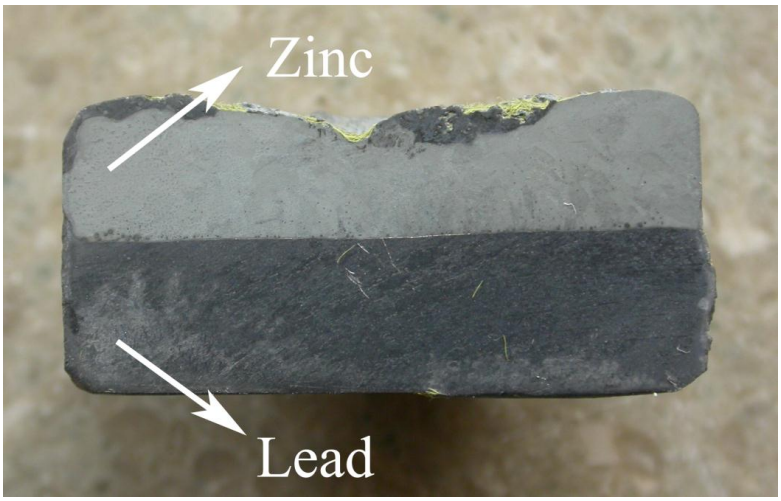

Figure 5.6. Cross-section image of polished surface of zinc-lead binary system.

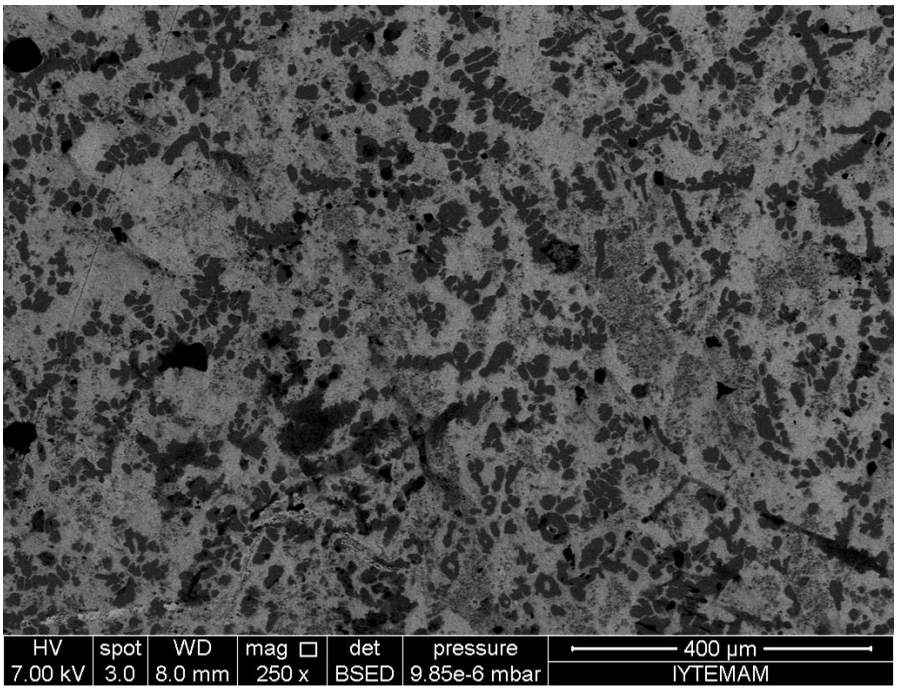

(a)

Figure 5.7. SEM images showing the microstructure of copper-lead binary system at (a) 250X and (b) 500X magnifications.

(cont. on next page)

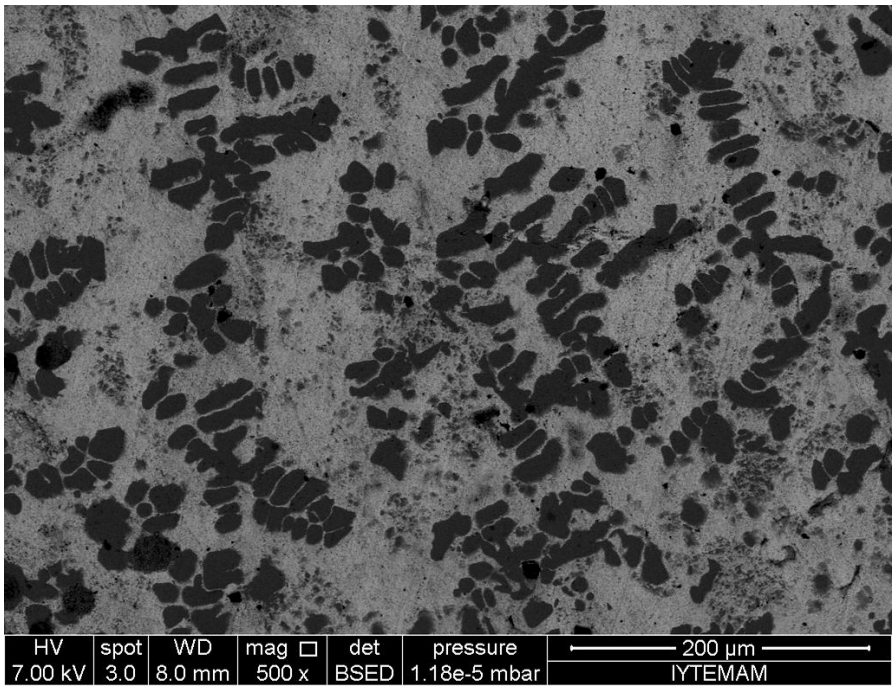

(b)

Figure 5.7. (cont.)

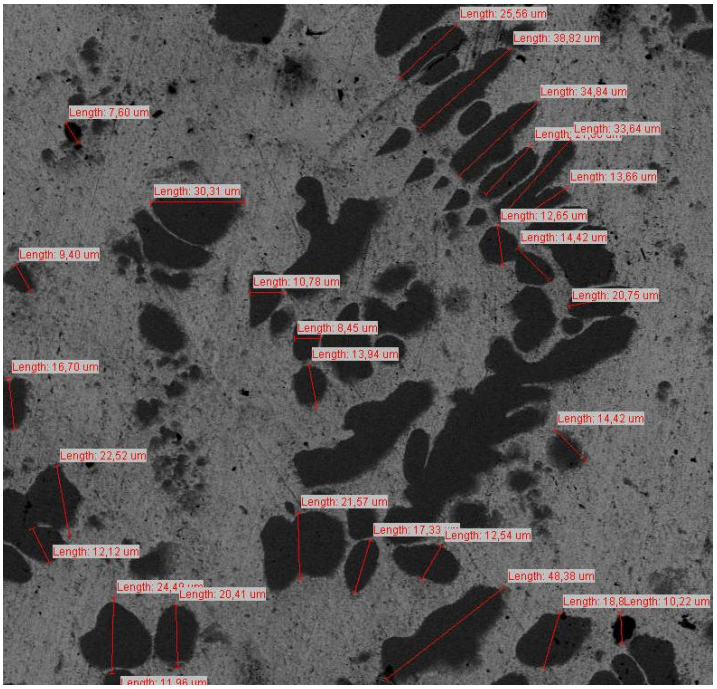

Figure 5.8. The sizes of copper phase.

5.2.2. Microstructure of Electrowon Samples

The surface micrographs of copper-lead binary alloy system after electrowinning are shown in Figures 5.9 and 5.10(a) and (b). Although small pores are seen, the surface is fully coated with a salt layer. EDX analysis shows that the salt layer contains 69 wt% Pb, 11 wt% S and 20 wt% O. The weights of the samples were recorded before and after the electrowinning experiments. The weight reduction is about 0.15 gr, which was the 22 % of copper in the sample. The stainless steel cathode electrode was coated with copper during electrowinning, proving the dissolution of copper.

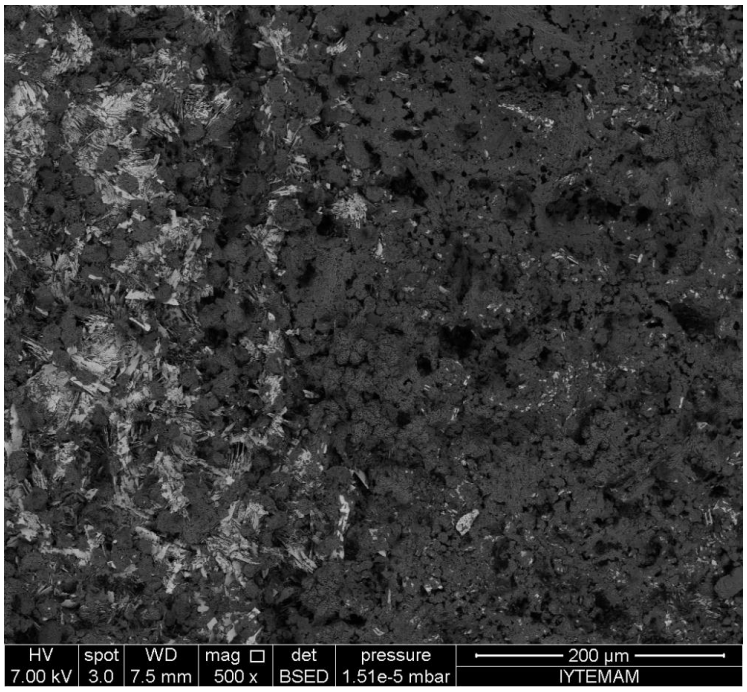

Figure 5.9. Porous surface of sample at 500X magnification after electrowinning.

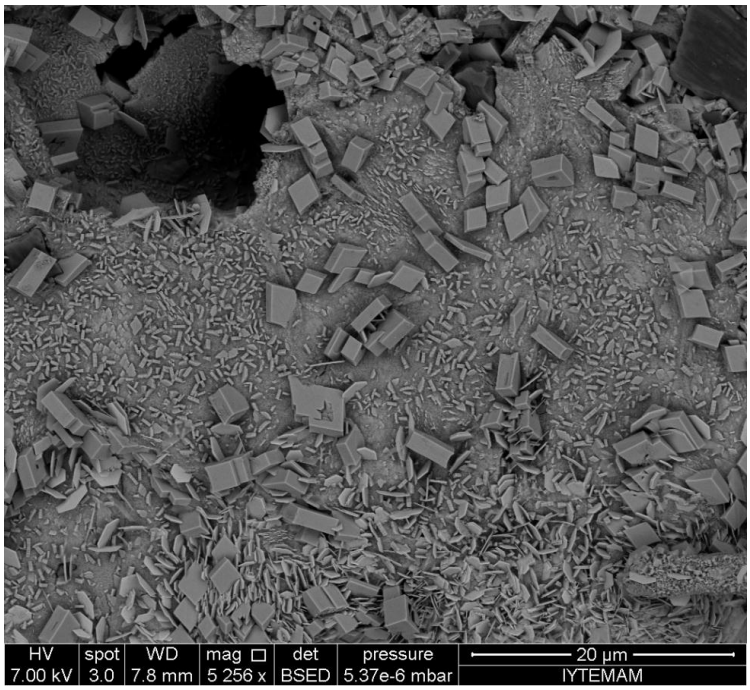

(a)

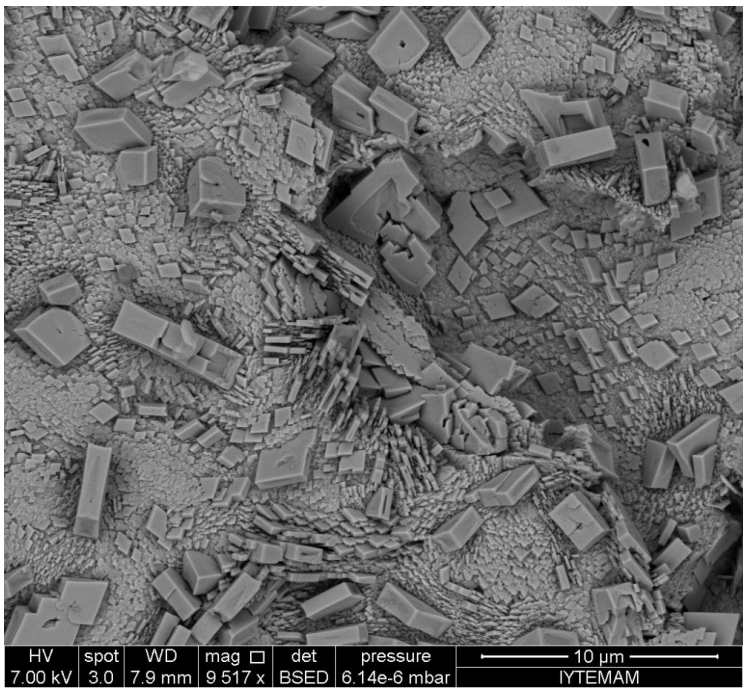

(b)

Figure 5.10. Salt layer on the surface at (a) 5256X and (b) 9517X magnifications.

5.3. Replication Methods

5.3.1. Silica Bead Replication

5.3.1.1. Structure of the Foams

Foam samples in two different porosities, 55% and 60%, and pore sizes 2 and 2.5 mm are prepared using silica beads. Figures 5.11(a-d) show the top view and side views of 55% porous foam sample before and after space holder removal, respectively. Figure 5.12(a-d) show the top view and side views of 60% porous foam sample before and after space holder removal, respectively. Each cell has interconnections with neighboring cells, confirming an open cell structure of the prepared foam samples. The space holder particles touching each other provide the interconnections between the pores and also with the mold surface. Microscopic analysis showed that each cell had 6 interconnections on the average. Figure 5.13(a) shows the SEM cell structure image of 60% porous and Figures 5.13(b,c) 55% porous foam samples. The size of the interconnection openings varies between 1 and 1.35 mm for 2.5 mm pore size sample, and 0.77 and 1 mm for 2 mm pore size sample. Small size precipitates are observed on the foam samples surfaces and interior of the cells (Figure 5.13(d)). These are lead (II) fluoride (PbF_2) precipitates [43] determined by EDX analysis and formed by the reaction between PbO and HF.

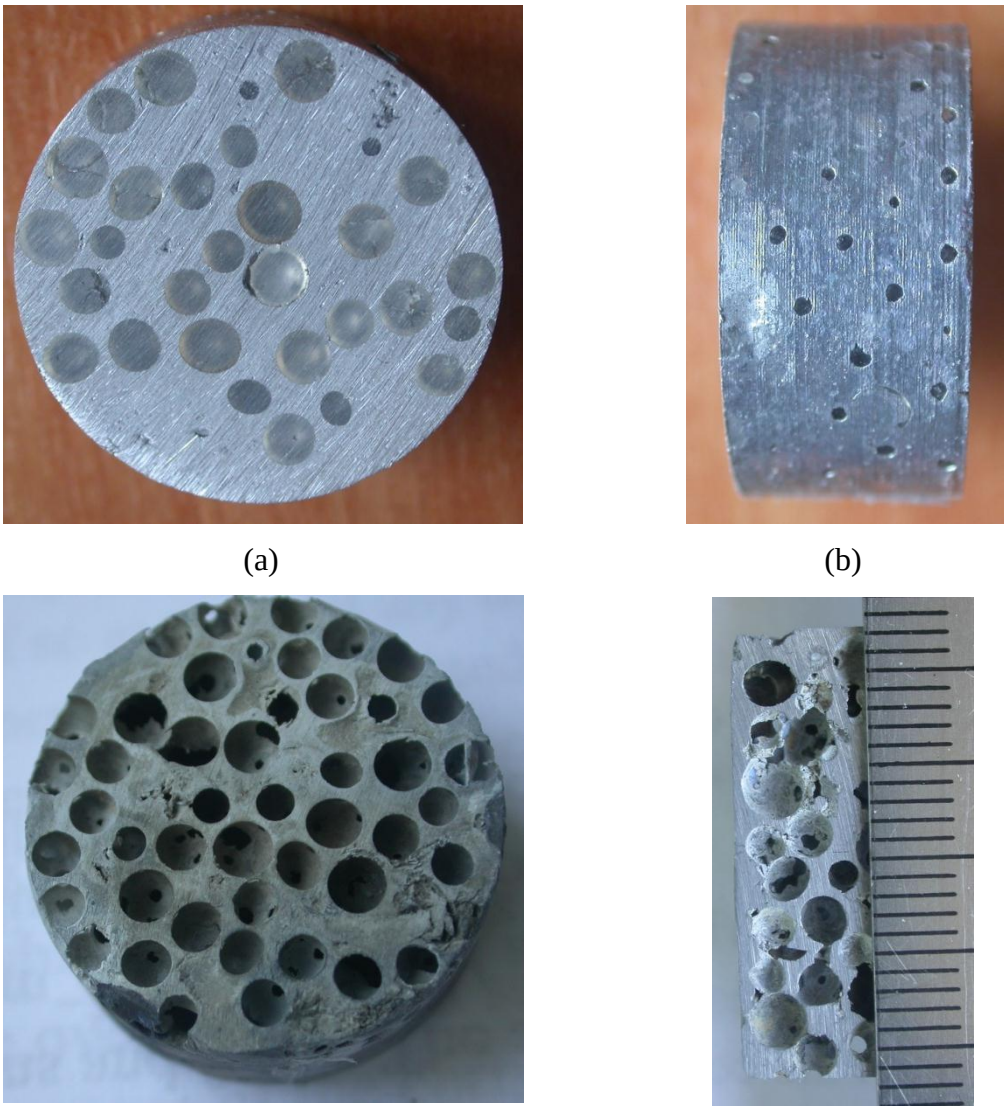

Figure 5.11. Foam sample with 2 mm pore size and 55% porosity (a) top view before space holder removal, (b) side view before space holder removal, (c) top view after space holder removal and (d) cross-section view after space holder removal.

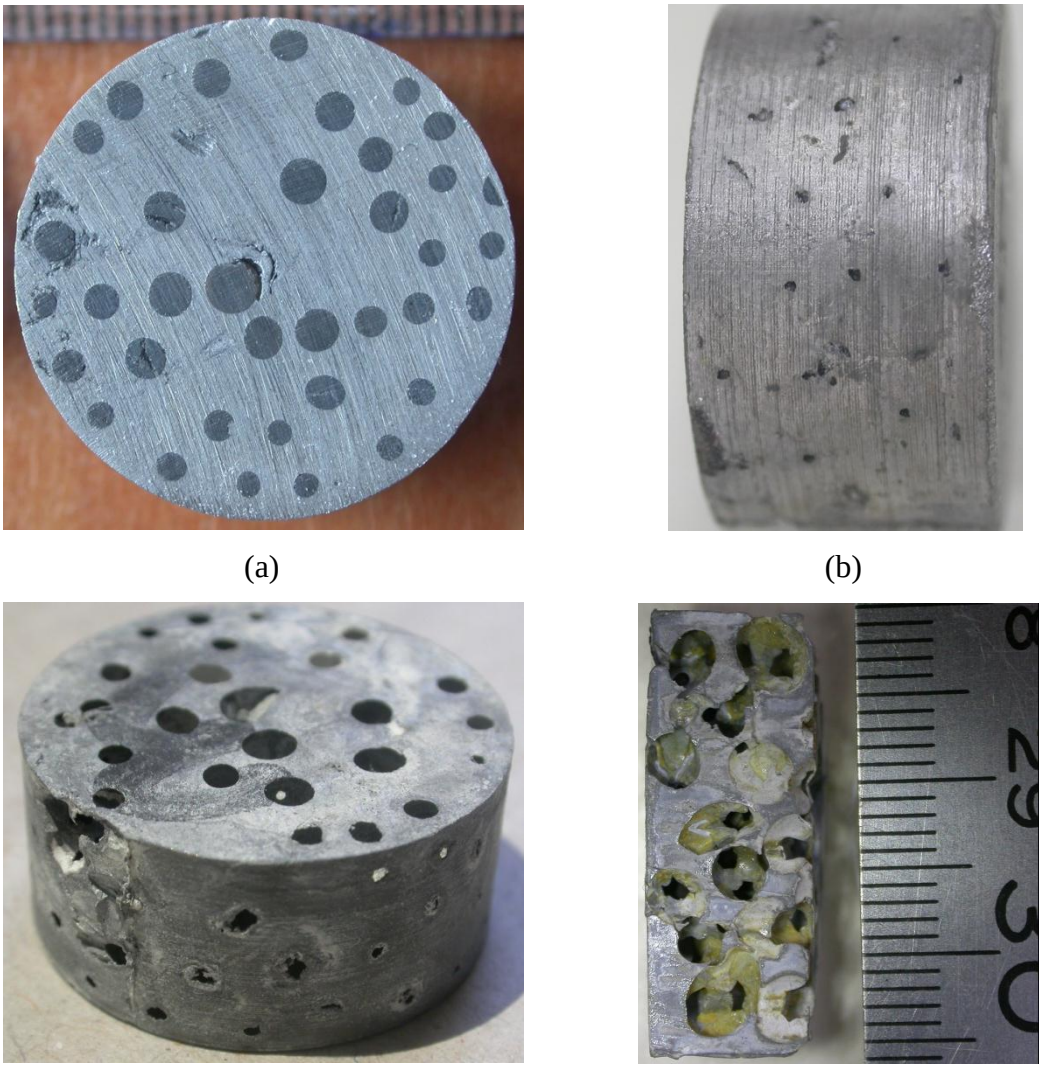

(a) (b)

(c) (d)

Figure 5.12. Foam sample with 2.5 mm pore size and 60% porosity (a) top view before space holder removal, (b) side view before space holder removal, and (c) after space holder removal and (d) cross-section view after space holder removal.

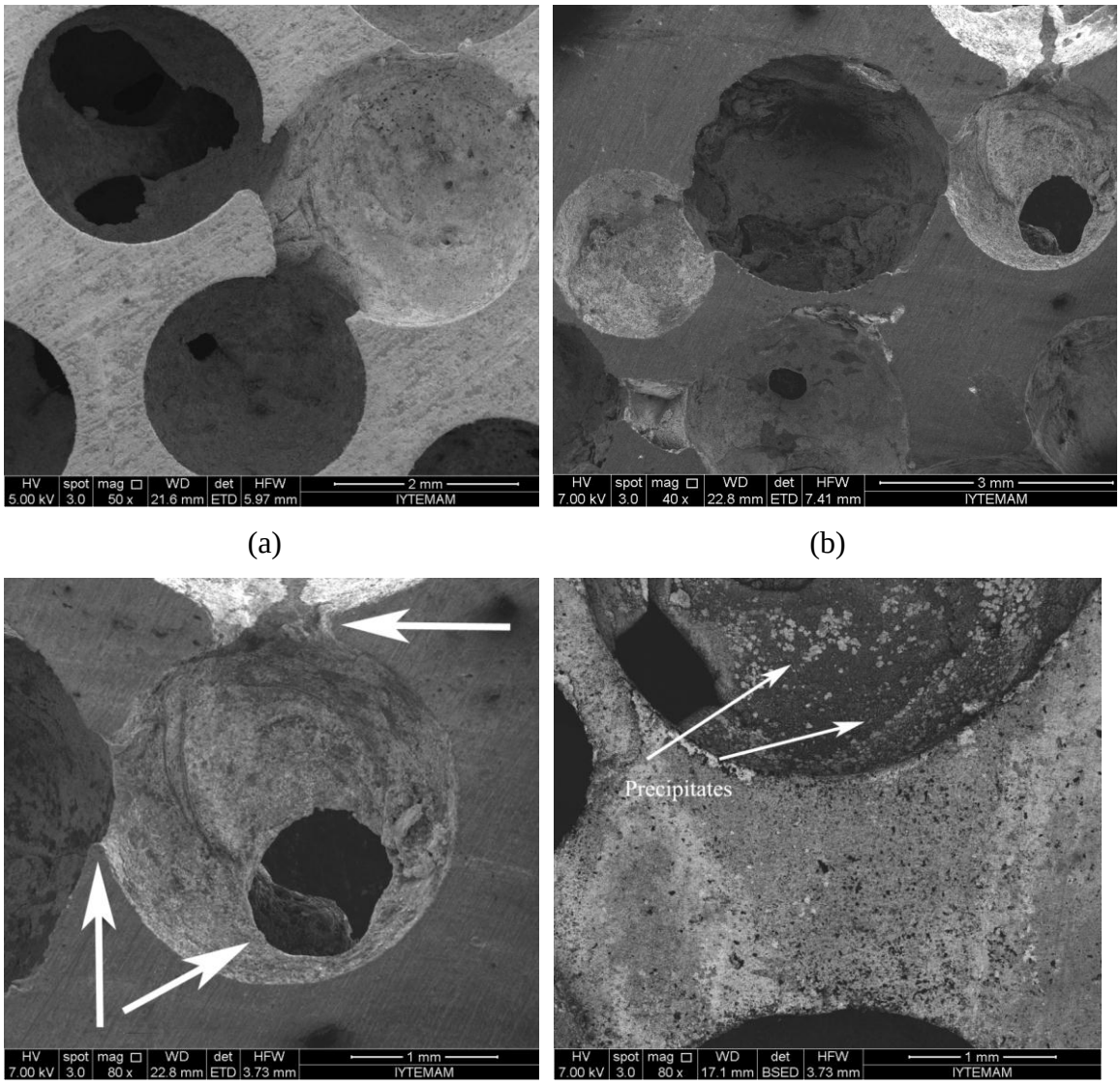

(a) (b)

(c) (d)

Figure 5.13. SEM images of (a) 60% porous foam, (b) 55% porous foam at 40X magnification, (c) 55% porous foam at 80X magnification and (d) PbF_2 precipitates on the cell walls.

5.3.1.2. Compression Mechanical Properties

Typical compression stress-strain curves of lead foams represent the characteristics of elastic-plastic foam deformation behavior as shown in Figure 5.14. The stress-strain curve composes of three distinct regions (shown by the numbers in Figure 5.14): (1) the linear elastic, (2) plateau and (3) densification regions. In the elastic region, the deformation is controlled by the elastic deformation of both cell edges and walls. In the plateau region, the deformation proceeds by collapse of cell

edges and walls. Following the plateau region, the stress increases rapidly in the densification region since the collapsed cell walls and edges are compressed all together. The collapse stress (σ_c) is calculated by proportional limit (inset of Figure 5.14). The foam elastic modulus (E) is calculated as the slope of the initial elastic region. The densification strain (ε_d) is calculated as the intersection of the tangents to the stress plateau regime and densification regime as in Figure 5.14 [44].

The compression stress-strain curves of lead alloy foams prepared using silica beads are shown in Figures 5.15(a) and (b). In the same figures, the compression stress-strain curve of bulk lead alloy is also shown for comparison. The collapse stress, plateau stress, densification strain and elastic modulus of the foams are also tabulated in Table 5.5. It is clearly seen in Figures 5.15(a) and (b) and Table 5.5 that as the porosity increases, collapse stress, plateau stress and elastic modulus decrease, while densification strain increases. Figures 5.16(a) and (b) show the cell deformation of a sample deformed up to 0.3 strains. The deformation is seen to proceed with cell wall buckling and rupture.

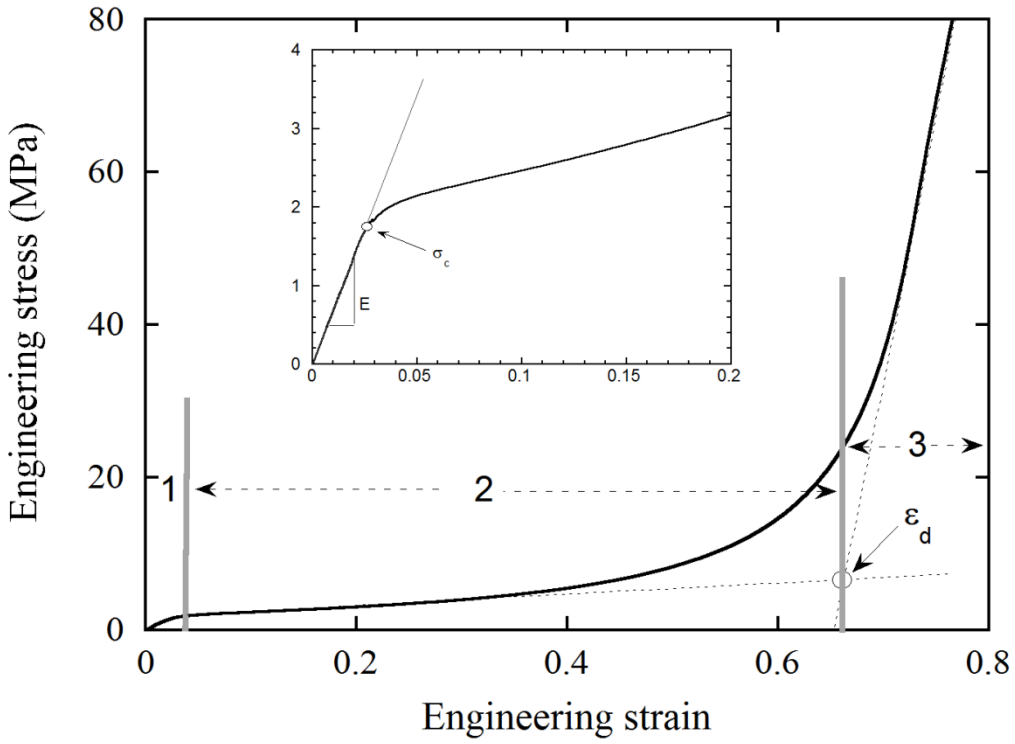

Figure 5.14. Typical compression stress-strain curves of lead foam prepared by replication method.

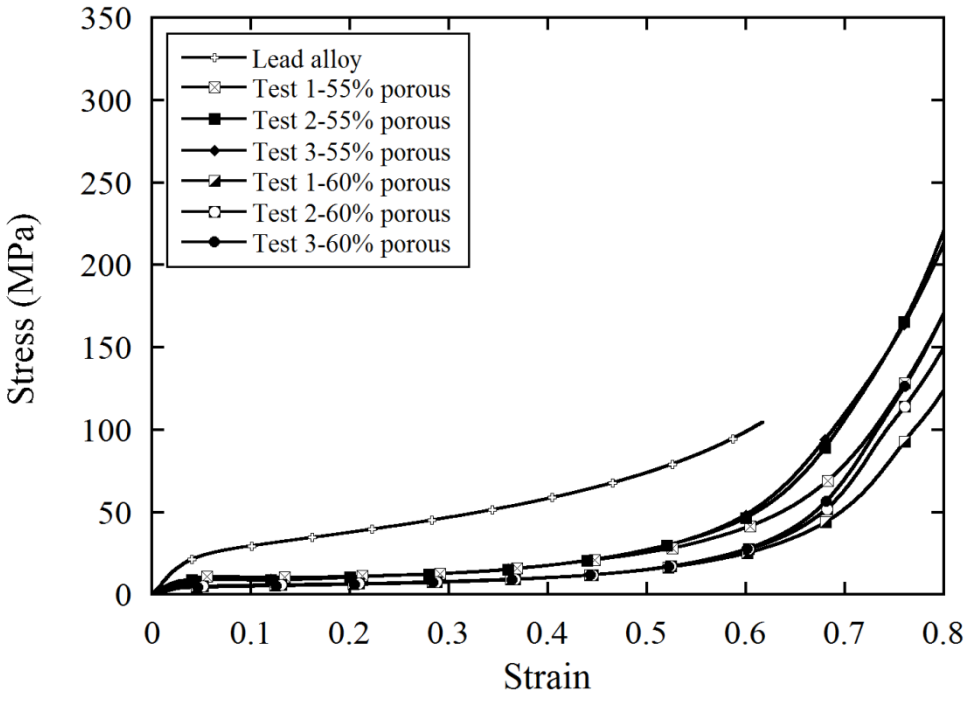

(a)

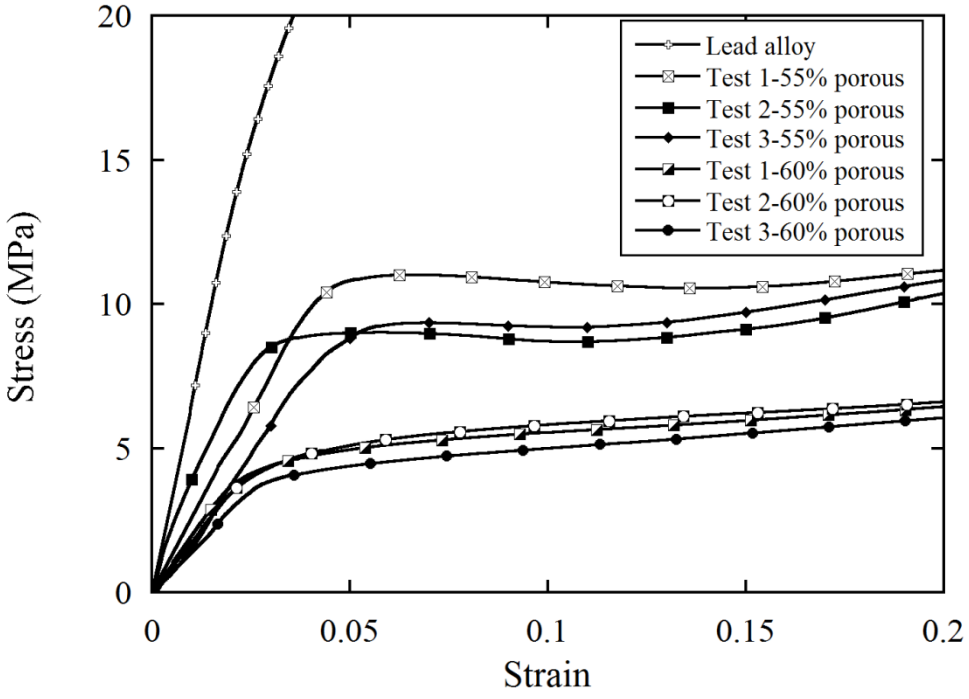

(b)

Figure 5.15. Compression stress-strain curves of foams prepared using silica beads: until about (a) 0.8 and (b) 0.2 strain.

Table 5.5. Compression properties of the foam samples prepared by the silica bead replication method.

Sample		Collapse Stress (MPa)	Plateau Stress (MPa)	Densification Strain	Elastic Modulus ($x10^{-3}$ GPa)
60% Porous 2.5 mm pore size	Test 1	3.71	7.59	0.656	199.32
	Test 2	3.69	8.05	0.642	174.30
	Test 3	3.69	7.65	0.642	139.29
55% Porous 2 mm pore size	Test 1	9.42	13.62	0.627	253.37
	Test 2	7.33	12.61	0.602	339.12
	Test 3	7.25	13.16	0.613	206.86

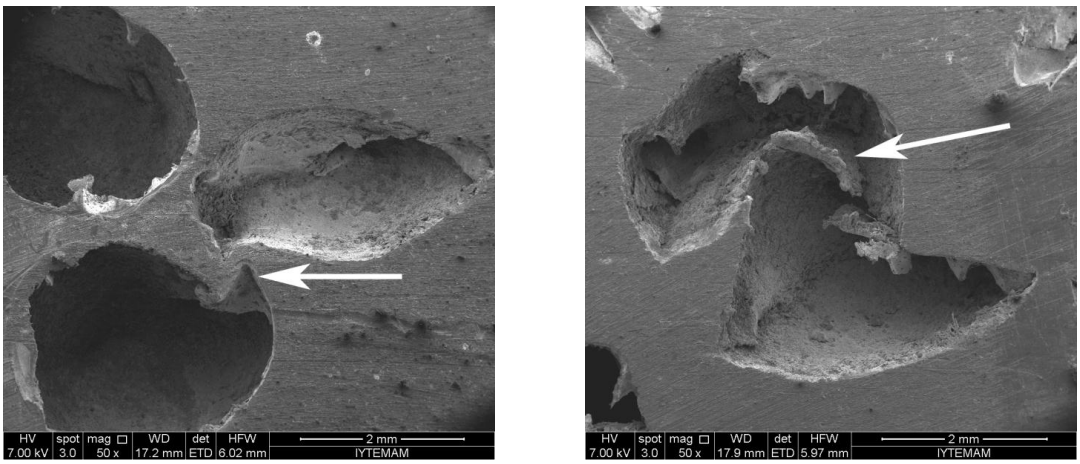

(a) (b)

Figure 5.16. (a) cell buckling and (b) rupture in lead foam prepared using silica beads.

5.3.2. Salt Replication

5.3.2.1. Structure of the Foams

Lead alloy foams prepared using salt particles had porosities of 65 and 74%. It should be noted that the maximum porosities which can be achieved using space holders are limited to the values below 80%. Figures 5.17(a) and (b) show SEM images of 74% porous foam sample before and after dissolution of space holder. In these pictures, cast lead alloy are seen white and salt particles are seen black. The liquid lead alloy is infiltrated efficiently through cell edges and nodes as seen in Figure 5.17(b). The foam cell sizes seen in Figure 5.19, are also relatively homogeneous. Figures 5.18(a-c) show the top and side views of 65% and 74% porous lead foams. The foams have

homogeneous cell size distribution. The SEM pictures of cells of 65% and 74% porous foam samples are shown in Figure 5.19. The pore sizes range between 241 and 565 μm for 65%, and 270 and 575 μm for 74% porous foams. Similar to the foams prepared using silica beads, foams prepared using salt particles have open cell structure: the cells have few interconnections with neighboring cells. The size of the interconnections is measured 180 and 213 μm for 65 and 74% porous foams, respectively.

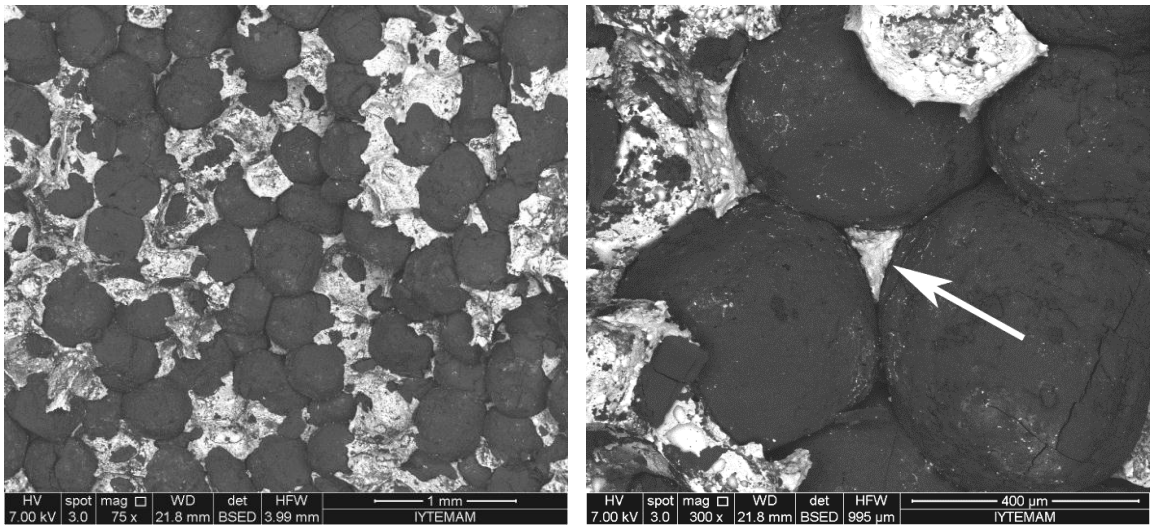

(a) (b)

Figure 5.17. SEM images of a 74% porous lead foams before salt particles removed; lead alloy is seen white and salt particles black.

(a) (b)

Figure 5.18. Salt replicated foams; 65% porosity (a) top, (b) side view and 74% porosity (c) top, (d) side view**.**

(cont. on next page)

(c)

(d)

Figure 5.18 (cont.)

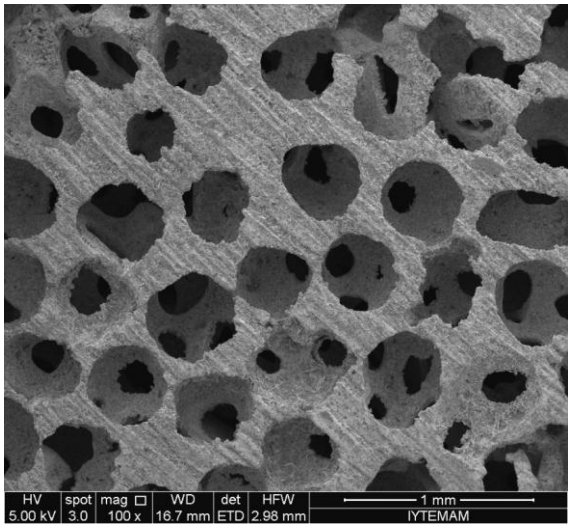

(a)

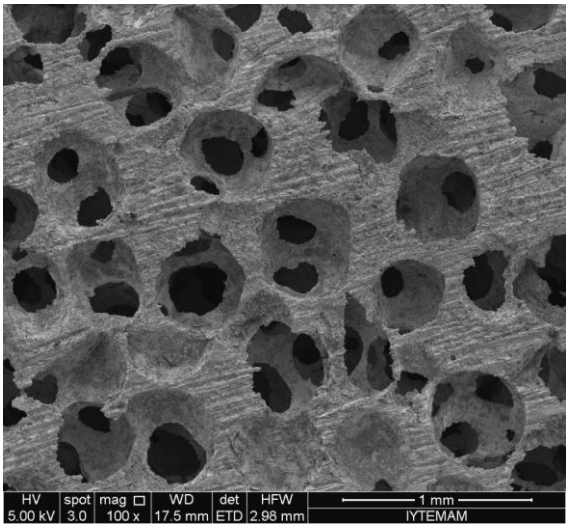

(b)

Figure 5.19. SEM images of the cells of (a) 65% and (b) 74% porous foams.

5.3.2.2. Compression Mechanical Properties

The compression stress-strain curves of lead alloy foams prepared using salt particles are shown in Figures 20(a) and (b). In the same figures, the compression stress-strain curve of bulk lead alloy is also shown for comparison. The collapse stress, plateau stress, densification strain and elastic modulus of foams prepared using salt are further tabulated in Table 5.6. Similar to foams prepared by silica beads, the collapse stress, plateau stress and elastics modulus of the foams prepared using salt particles

decrease as the porosity increases. Figures 5.21(a), (b) and (c) show the optical microscope images of a foam sample before the compression and after compression testing at 0.07 and 0.14 strain, respectively. Figure 5.22 shows the SEM image of a foam sample compressed until about 0.21 strains. It is clearly seen in these figures the deformation proceeds with the cell wall buckling and cell wall rupture.

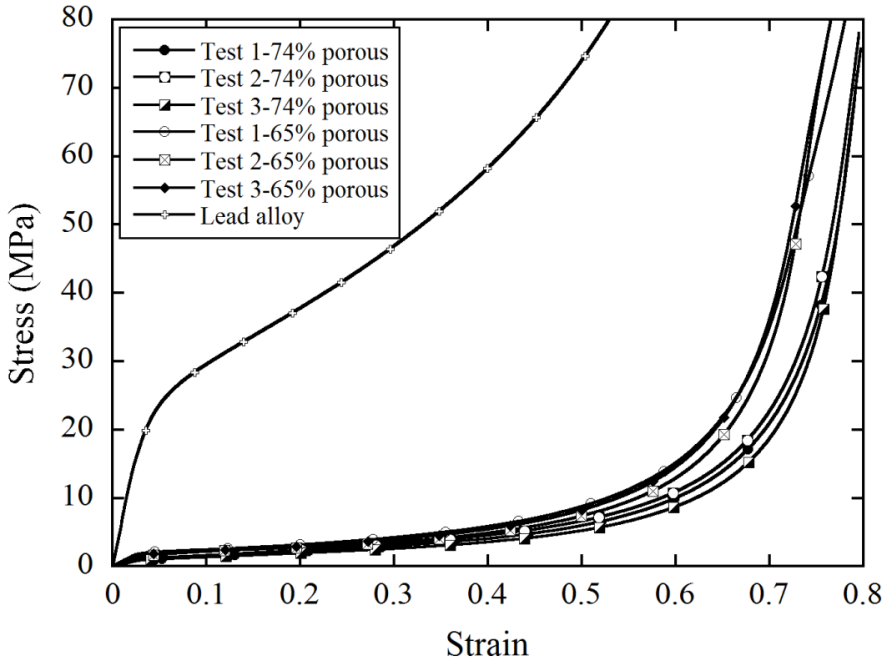

(a)

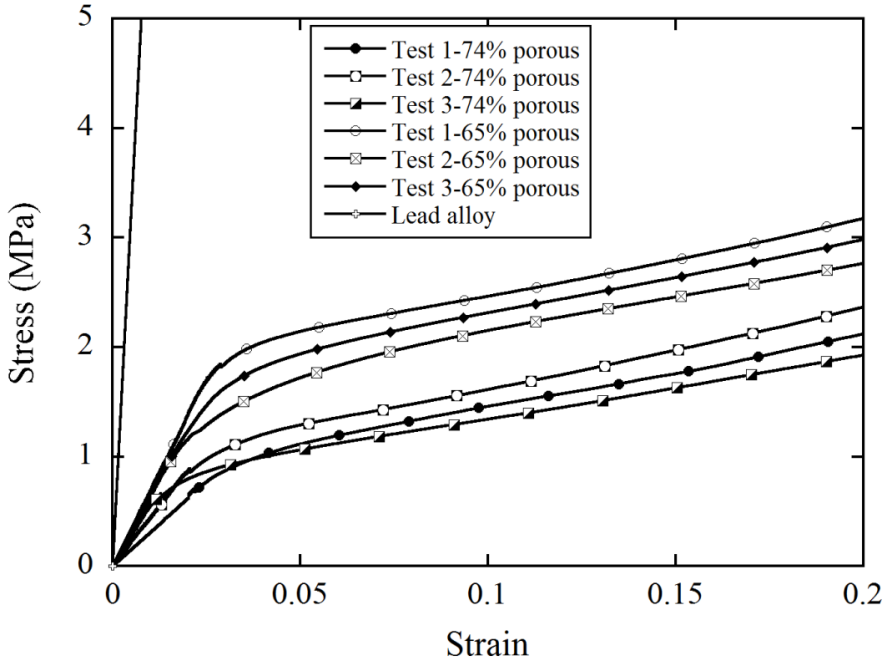

(b)

Figure 5.20. Compression stress-strain curves of foams prepared by salt particles: until about (a) 0.8 and (b) 0.2 strain.

Table 5.6. Compression test results of 65 and 74% porous samples.

Sample		Collapse Stress (MPa)	Plateau Stress (MPa)	Densification Strain	Elastic Modulus (x10^{-3} GPa)
65% Porous 440 µm pore size	Test 1	1.681	4.141	0.655	70.03
	Test 2	1.149	3.538	0.664	63.31
	Test 3	1.318	3.844	0.651	64.79
74% Porous 440 µm pore size	Test 1	0.831	2.936	0.729	31.53
	Test 2	0.886	3.246	0.716	44.64
	Test 3	0.664	2.472	0.731	57.19

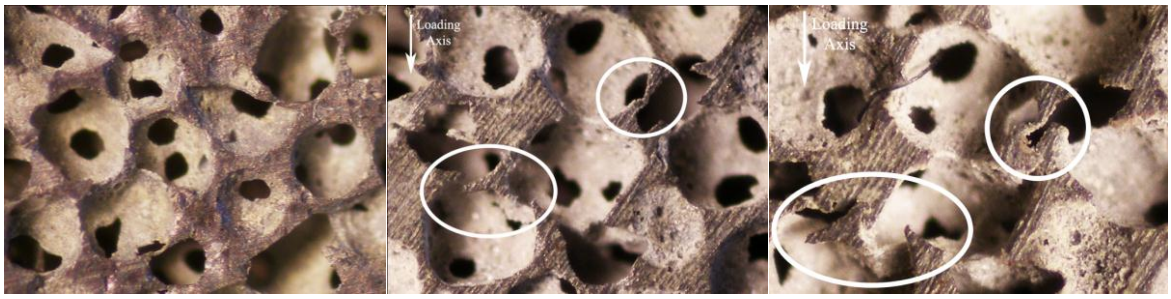

(a) (b) (c)

Figure 5.21. Optical microscope images of (a) undeformed and the deformed foam samples (b) 0.07 strain and (c) 0.14 strain.

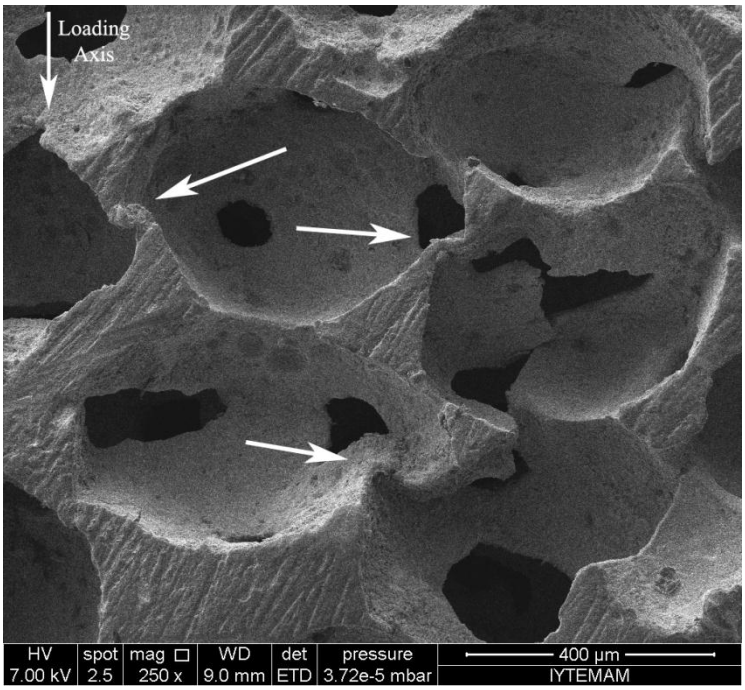

Figure 5.22. SEM image of the 0.21 strains deformed foam sample.

CHAPTER 6

DISCUSSION

6.1. Powder Metallurgy Route

Open cell lead foams were successfully prepared through powder metallurgical routes using a space holding material. The possible space holders include ammonium bicarbonate and urea. Ammonium bicarbonate has relatively low decomposition temperature, about 200°C. The decomposition temperature of urea, 600°C, is well above the melting temperature of lead, 327°C. The decomposition reactions of ammonium bicarbonate and urea are sequentially given as

$$NH_4HCO_3 \rightarrow NH_3 + H_2O + CO_2 \quad (6.1)$$

$$(NH_2)_2CO + H_2O \rightarrow 2NH_3 + CO_2 \quad (6.2)$$

Foam preparation started with the compaction of homogeneous mixture of metal powder and space holders. A binder is generally used to facilitate a higher particle packing. As lead powder particles are easily deformed and efficiently packed to the green densities up to 99%, no binder is used in the compaction stage. After the compaction, the compression test samples were prepared through core drilling before the space holder removal stage. The core drilling after space holder removal stage caused the deformation of the compact; although, the applied stress was kept as low as possible during core drilling. In core drilling before space holder removal stage, the space holder particles minimized the deformation of the pores by supporting the pores.

The porosities of green compacts varied between 44.6 and 51.0% depending on the applied compaction pressure. As the compaction pressure increased, the porosity level decreased. The powder mixture was prepared in order to obtain 50% porosity; however, few samples had higher porosities (51.4%) than the targeted porosity level. This was likely due to the insufficient compaction pressure (71 MPa). In contrast, applying excess pressures resulted in lower porosities (44.6%). In the compaction with

excess pressure, the carbonate particles changed their original size and shape and were elongated normal to the compaction direction. Excessive pressures also caused the smashing of the space holder particles. The initial particle size of the space holders were between 315 and 500 μm; however, the pore sizes of the foams measured from SEM images varied between 231 and 121 μm depending on the applied compaction pressure. As the compaction pressure increased, the pore size decreased. Considering the targeted green density and the extent of damage on the carbonate space holder particles, the optimum compaction pressure is about 100 MPa.

Compression test showed an elastic-brittle foam deformation characteristic. Initially, the samples were deformed elastically; then failed catastrophically rather than showing an extended plateau region which was the common deformation characteristic of the foam produced by powder metallurgy [45]. The presence and/or formation of the oxide layer around the particles may lead to weak bonding between the particles. Lead can be oxidized easily at ambient conditions. The white lead particles covered with the gray oxide layer in Figure 5.4 are lead oxide.

As the compaction pressure increased, the density of the foam increased; hence, the collapse stresses increased. The collapse stresses of the foams compacted at 71 and 142 MPa and sintered at 261°C increased from 2.62 to 6.2 MPa and 3.54 to 8.41 MPa, respectively. Increasing the sintering temperature from 261°C to 286°C and to 300°C resulted in increase of the collapse stress from 8.41 to 8.57 and to 9 MPa, respectively. Sintering also increased the failure strain of the samples by improving the bonding between particles. Green body samples showed catastrophic failure at 0.017 strains while the failure strains of the samples sintered at 261, 286 and 300°C were 0.018, 0.023 and 0.033, respectively.

The equilibrium partial pressure of oxygen for the oxidation reaction of lead using carbon as reducing agent at 300°C is about the 10^{-31} P_{O2} atm (Figure 6.1). This pressure of oxygen cannot be practically achieved since the lowest vacuum level achieved by any known vacuum pump is higher than the equilibrium oxygen pressure. Therefore the foam produced by the powder metallurgy is expected to have very low electrical conductivity due to oxide formation.

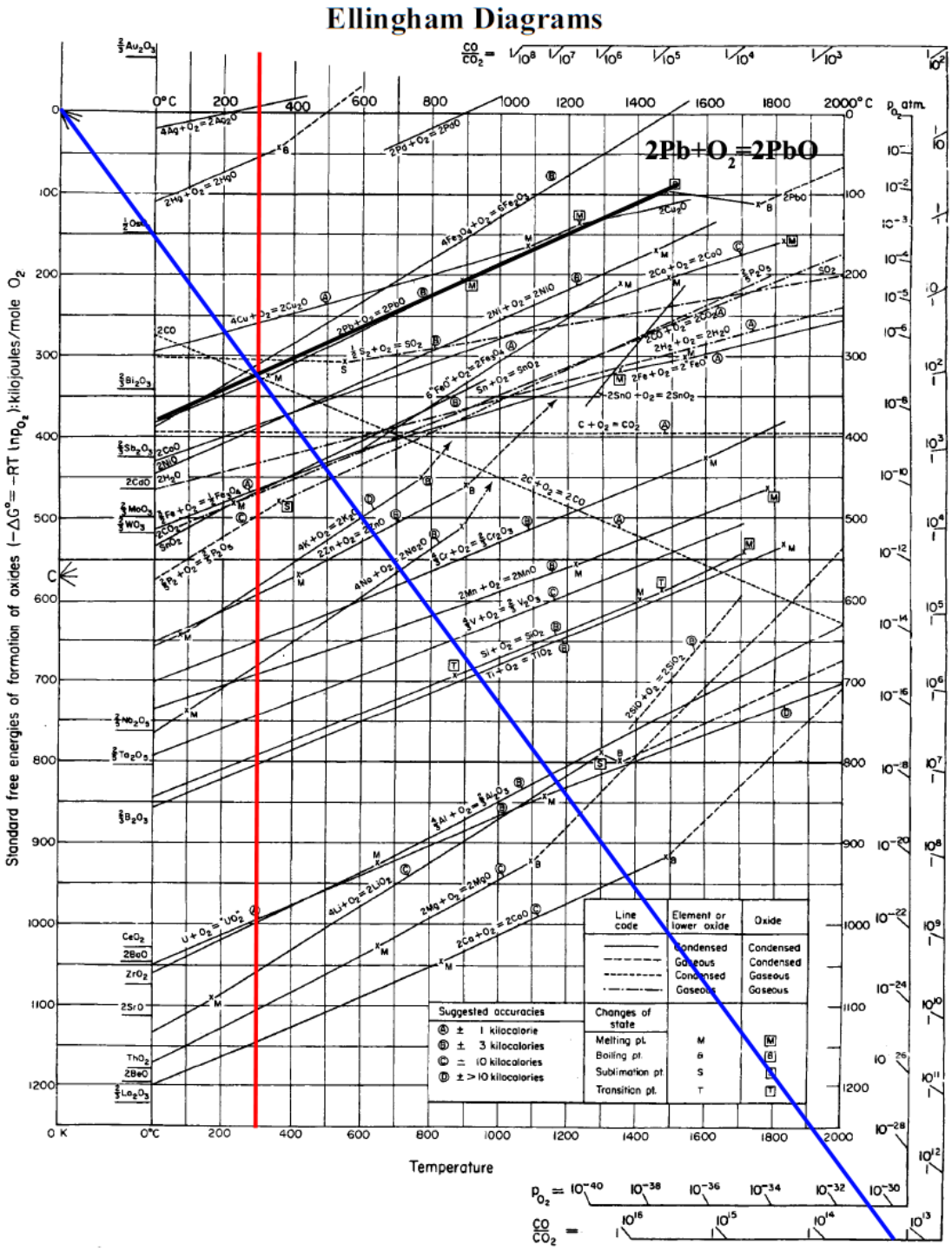

Figure 6.1. Ellingham diagrams [46].

6.2. Electrowinning Method

Electrowinning of the immiscible secondary phases from the matrix might be a promising method for lead foam production. There are limited numbers of immiscible elements for lead, only copper and zinc. As the melting point of the copper is relatively high, the melting process must be performed at a relatively high temperature. However, high processing temperatures result in change in the stoichiometry of the metal elements caused by the evaporation of lead. The weight of lead melt was reduced by 15% after melting and casting.

Although electrowinning ended up with a porous surface, the cross-section of the samples could be investigated as the cutting of the samples smeared the cut surfaces. During electrowinning experiments, the applied current was kept constant for all samples at 1.4 A which provided the maximum current efficiency during electrowinning [39]. With use of highest efficiency current only the 50% of the copper was reduced during electrowinning.

The surface of the samples was covered with crystal salt layer after electrowinning. The salt layer contained 69 wt% Pb, 11 wt% S and 20 wt% O, which was matched with the chemical composition of lead sulfate (68.32 wt% Pb, 10.57 wt% S and 21.10 wt% O [42]). Additionally the crystal structure of the salt particles also matched with that of lead sulfate, monoclinic ($a \neq b \neq c$, $\alpha = \beta = 90° \neq \gamma$) structure. This salt layer was seen in white color in SEM (back-scatter mode) because of the higher molecular weight of $PbSO_4$ than Pb and PbO. Lead sulfate crystals are essential component of lead-sulfuric acid batteries and forms during discharge cycles, especially application of overpotential causes the formation of lead sulfate as [47],

$$PbO + SO_4^{2-} + 2H^+ \rightarrow PbSO_4 + H_2O \qquad (6.3)$$

Lead sulfate can also form by the reaction between lead oxide and concentrated sulfuric acid under warm condition [42]. Lead sulfate can be dissolved in concentrated sulfuric acid [42], which is the electrolyte of the lead-acid batteries.

This method is applicable for the manufacturing of battery electrode, if the homogeneous porous foam plates can be produced with an appropriate secondary phase material. However, the main problem with this method is the lead evaporation. Because

of this evaporation, it is hard to control the stoichiometry of the melt and also the emission of lead is highly toxic for the environment and health. To prevent the lead emission, melting must be done in a closed system.

6.3. Replication Method

6.3.1. Silica Bead Replication

Foams with two different porosities were prepared using silica beads; 55 and 60%. Silica beads with 2 mm average diameter resulted in 55% porous foams, while 2.5 mm average diameter 60% porous foams. Higher porosity foams could not be prepared using 2 mm particles. The density of the silica bead depends on the producer. Although the density of 2.5 mm particles was provided by producer, the density of 2 mm particles was specified. The density of the beads could also not be determined with Archimedes method due to high affinity of beads to water absorption. In addition, the volume of the beads cannot be calculated geometrically because of the irregular shapes of the beads. The foams of 55% porosity were prepared by the trial and error method of different amounts of beads. However 60% porosity foams were prepared based on the calculations given in Chapter 4. The use of bigger space holder particles (2.5 mm) resulted in bigger node regions that were smaller than the space holder particles. To increase the porosity level, these node regions need to be filled with space holder particles instead of molten lead; however these regions cannot be filled with the used space holder particles, due to narrow distribution of silica beads. The beads were not small enough to fill more space in the mold, thus if the beads with broader size distribution are used higher porosity levels can be achieved.

During the microstructure analysis of the foam samples after space holder replication, PbF_2 precipitates on the cell walls are seen in Figure 5.13(d). it was previously mentioned that PbF_2 layer covering the surface did not cause passivation of the lead electrode during charge and discharge [48]. The solubility of PbF_2 in water was previously found as 0.66 g/l (2.7 mMol/l) [42]; therefore, this layer can also be dissolved in water.

6.3.2. Salt Replication

The properties of lead acid batteries are closely related with the electrode design. The use of porous electrodes increases the discharge current density, utilization efficiency and power density. The improvements of these properties depend on the surface area of lead electrode. It was shown that the surface area of foam was inversely related with the size of the strut diameter and the window diameter [49]. The cell size and strut diameter were shown to be directly proportional to each other; increasing cell size increased the strut diameter [50]. Lead foam using smaller size salt particles as space holder, with the average particle size of 440 μm and 381 μm, were prepared to reach higher porosity levels. The use of smaller particles prevented the completely penetration of molten metal. As the particle size decreases the strut diameter becomes smaller [50] and higher forces need to be applied for the infiltration of the molten metal into empty spaces [12].

The porosity of foam needs to be increased in order to increase the surface area. However there is a limit for the maximum achievable porosity level in the infiltration method. The maximum porosities which can be achieved by using space holders are limited to values below 80% [16]. The highest foam porosity obtained using salt particles is 74%. This value also matches well with the densest packing of FCC and HCP crystal structures, 0.74. The lowest porosity level obtained with salt replication is 65%. Foams with lower porosity levels could not be produced with this method. During the replication process in mold, salt particles could not be mixed with all of the liquid metal and placed at the bottom of the mould. As a result of this, a dense lead layer forms at the top of the mold as shown in Figure 6.2.

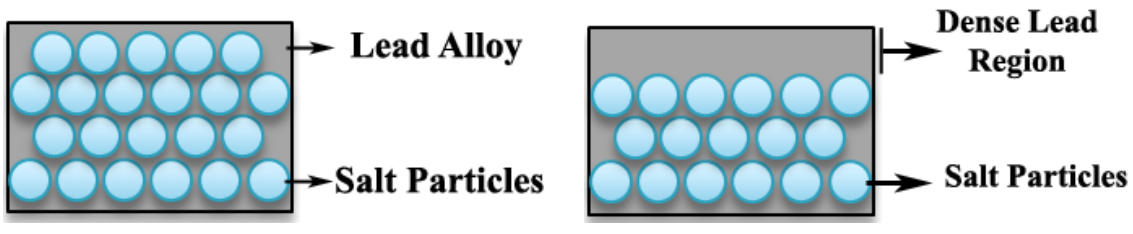

Figure 6.2. Schematic representation of (a) successfully prepared 65 and 74% porous foam structure and (b) unsuccessful 60% porous foam structure before space holder removal process.

6.3.3. Mechanical Properties of Replicated Foams

The compression mechanical properties of open cell foams are function of porosity and pore size. Jiang et al. [45] investigated the effects of pore size and porosity level on the mechanical properties of open cell aluminum foams. The collapse and plateau stresses were shown to decrease with either increasing porosity or the decreasing pore sizes. Similar effects of porosity and pore size on the collapse and plateau stresses were detected in lead foams [31]. Lead foams produced by the replication of the silica beads also showed similar behavior. As the porosity increased from 55 to 60% and pore size increased from 2 mm to 2.5 mm, the collapse stress decreased from 8 to 3.7 MPa and plateau stresses decreased from 13.13 to 7.76 MPa. The collapse stress depends on the cell edge thickness; as the cell edge thickness decreases, the load carrying cross section area decreases and hence the edge fails by buckling at relatively lower stresses. The cell edge thickness varies with porosity and pore size. As the porosity increases the edge thickness becomes thinner and as the pore size increases the cell edge become thicker. The foams samples produced by salt replication process had higher porosities and smaller pore sizes than the foams produced by silica bead replication. The increasing porosity and decreasing pore sizes resulted in thinner cell edges, leading lower collapse stresses. The collapse stress values were 0.79 and 1.38 MPa for the foam samples having 65 and 74% porosities and 440 μm average pore size, respectively.

The elastic modulus of the bulk lead alloy is $673x10^{-3}$ GPa. The elastic modulus of foams changes with the density. As the porosity of foam increases, the elastic modulus decreases [12, 51]. Lead foam samples showed similar behavior; elastic modulus decreased with the increasing porosity. Elastic modulus decreased from $266.45x10^{-3}$ to $44.45x10^{-3}$ GPa as the porosity increased from 55 to 74%.

The deformation in the collapse region proceeded with cell edge crushing over the cell walls and cell wall buckling, indicating typical deformation behavior of elastic-plastic open cell foam deformation (Figure 5.16). The collapse started initially at the interconnection regions and thin cell walls were observed to occasionally rupture. A similar foam deformation mechanism was also seen in the foam samples prepared with the salt replication (Figure 5.21). The deformation proceeded with cell wall bending and

tearing of cell walls. During densification the foam sample density approaches the bulk material. As the porosity level increased, the densification strain increased [45, 52].

6.4. Mechanical Properties

The mechanical properties of the porous materials are predicted by Gibson and Ashby model given as [51]

$$X_f = X_b C\left(\rho^*\right)^y \tag{6.4}$$

Where, X_f is the collapse stress or elastic modulus of the foam, X_b is the yield strength (collapse stress) or elastic modulus of bulk alloy, C is a constant, y is the exponential constant and ρ^* is the relative density, which is defined as

$$\rho^* = \left(\frac{\rho_f}{\rho_b}\right) \tag{6.5}$$

where, ρ_f and ρ_b are the density of foam and foam cell wall alloy respectively. The values of y for open cell foams are 1.5 and 2 for collapse stress and elastic modulus respectively. The yield strength (collapse stress) and elastic modulus of lead alloy used were determined experimentally and found sequentially as 15.3 MPa and 0.673 GPa. The variation of the elastic modulus and collapse stress of lead foam with relative density is shown in Figure 6.3. The collapse stresses of the foams prepared by the powder metallurgy with 48% porosity are shown in the same figure by a circle. The fitting parameter of C for collapse stress and elastic modulus of the prepared foams are found 1.15 and 1.12, respectively. The value of C for the elastic moduli of open cell foams was shown 1 [51], matching the predicted value of C for the prepared lead alloy foams. While the value of C predicted for collapse stress is higher than the reported C value, 0.3. The imperfections such as curved, wrinkled and missing cell walls, voids on the cell edges and cell walls and non-uniform density may lead to discrepancy between experimental and theoretical collapse stress values. The densification strain of open cell foams is described with the following scaling relation [52],

$$\varepsilon_d = 1 - \alpha_0 \left(\rho^*\right)^{1/2} \tag{6.6}$$

where, α_0 is a constant or particular foam structure. The fitting of the densification strain of the studies foam gives a value of 0.56 for α_0 (Figure 6.3). Depending on the cell wall topology, the value of α_0 was reported vary between 0.7 and 1.55 for open cell foams. The variations between the methods of determination of densification strain may lead to differences between the predicted values of α_0. The densification strains of commercial metallic foams ranged between 0.4 and 0.9 [13] and the densification strains of the prepared foams were within this range.

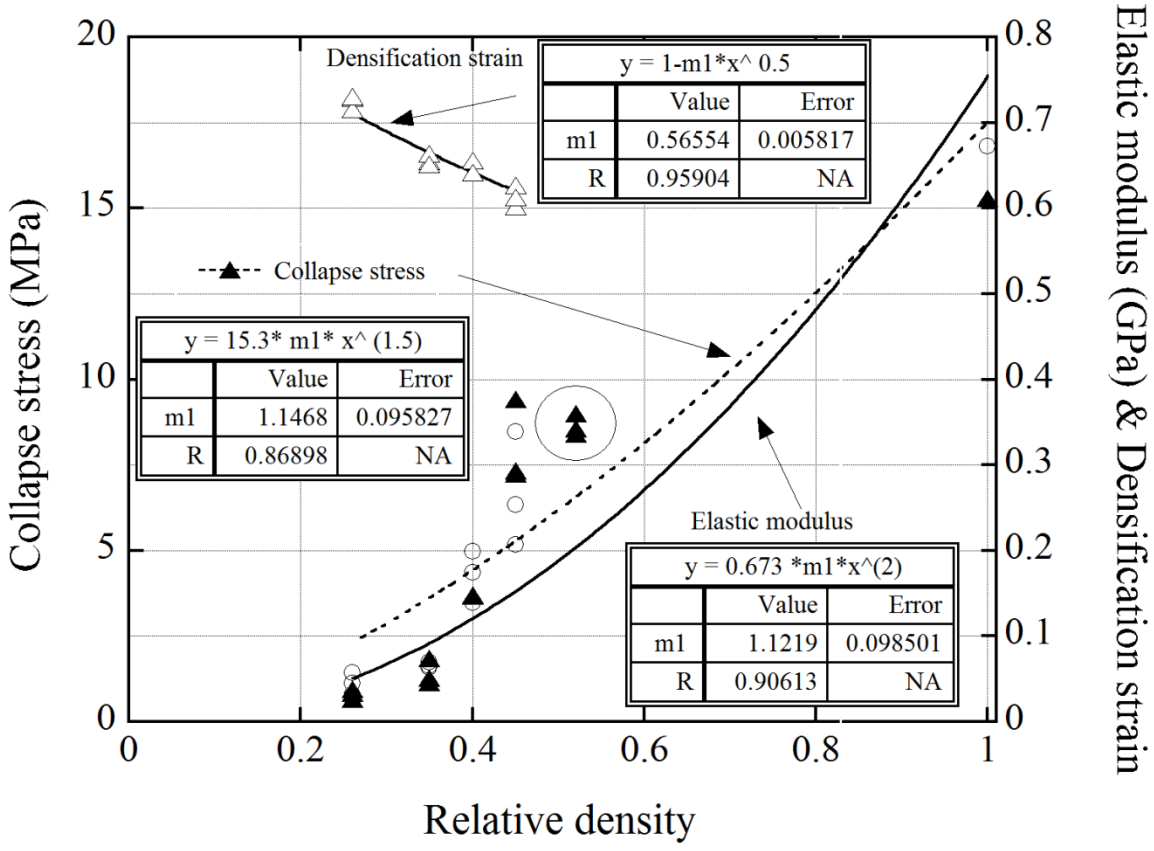

Figure 6.3. Collapse stress, elastic modulus, and densification strains as function of relative density.

CHAPTER 7

CONCLUSIONS

In this experimental study, 4 different methods were investigated to prepare lead alloy foams which can be used as an electrode in lead-acid batteries to increase the battery performance. In the first powder metallurgy method, foams were prepared by mixing of lead powder and ammonium bicarbonate space holder particles with 50 volume% ratio. The powder compacts were heat treated at 200°C in order to remove the space holder prior to sintering of pellets at 261, 286 and 300°C temperatures for 2 h. In the second process, the powder compacts were prepared with TiH_2 blowing agent and foamed at 450°C. In the third method, lead alloy was melted and casted with an immiscible element. After solidification, the immiscible metal was removed through electrowinning. In the last method, molten lead alloy was infiltrated around the space holder particles, and then the space holders were removed. The followings can be concluded for powder metallurgical route;

- The decomposition of ammonium bicarbonate completed at a relatively lower temperature but the decomposition temperature of urea was higher than the melting point of lead.
- The applied pressures during compaction affects the microstructure and porosity of the foam, as the compaction pressure increased, space holder particles were deformed excessively and resulted in reduced porosity. However, the compaction at 71 MPa resulted in higher porosity than the calculated value because of the loose packing of particles.
- Compression stress-strain tests showed that collapse stresses and failure strains of the foam samples were highly dependent on the compaction pressure and sintering. As the compaction pressure increased and with the sintering, the collapse stress and failure strains increased by 45% and 57%, respectively.
- Sintered samples showed elastic-brittle compression characteristics due to the lack of bonding between particles caused by the oxide film formation around lead particles.

- Powder compact melting method was found to not applicable because the blowing agent decomposed far after the melting of the lead powders.

The following can be concluded for the electrowinning process;

- The lead powder compacts containing TiH_2 blowing agent were not foamed at 450°C. Since the lead powder compact melted long before the decomposition of TiH_2, the viscosity of lead was presumed to be not sufficient for the stable bubble growth.

The followings can be concluded for electrowinning process;

- Copper and zinc were identified as forming immiscible liquid phases with lead.
- There was phase separation between lead and zinc after solidification of the melt however copper distributed in the forms of lamellar or droplets in the lead matrix.
- Since melting was performed at very high temperatures, the stoichiometry of the mixture was altered due to the evaporation of lead.
- Only 50% of the copper was collected during electrowinning.
- It was observed that the surface of the samples was covered with a $PbSO_4$ layer, which was presumed to have any negative effect on the efficiency of lead-acid batteries.

The followings can be concluded for replication process;

- By using two different sizes of silica beads, 2 and 2.5 mm, 55 and 60% porous foams were prepared.
- Since the space holder particles touched each other before infiltration, during space holder removal process hydrofluoric acid dissolved completely space holders.
- Microstructure characterizations showed that the pore structure was uniform with the average pore sizes of 2 and 2.5 mm.
- During space holder removal HF reacted with lead alloy and produced small size PbF_2 precipitates on the cell walls.
- Compression stress-strain tests showed that as the porosity increased, the elastic modulus, collapse stress and plateau stress decreased.
- The compression deformation proceeded through cell edge crushing and cell wall buckling.

- Lead foams with 65 and 74% porosities were successfully prepared using salt particles with a 440 μm average size.
- Salt particles were completely dissolved in boiling water with a vacuum assistance without any evidence of precipitate formation.
- Compression stress-strain results showed elastic-plastic characteristic.
- The deformation mechanism was the same with the foams prepared by the silica bead replication.
- The compression stress-strain elastic modulus, collapse stress and densification strain were fitted with the scaling relations. The fitting parameters of elastic moduli were found slightly higher than the literature. The fitting parameter of collapse stress was 73% higher than in literature, which was attributed to the imperfections in microstructure. While, the fitting parameter of the densification strain was in the range of the reported values.
- Based on the mechanical properties and microstructure, salt replication process was found to be the most suitable method to produce open cell lead foams for lead acid batteries.

REFERENCES

[1] L. J. Gibson, *Cellular solids : structure & properties / Lorna J. Gibson, Michael F. Ashby*. Oxford [Oxfordshire] ; New York :: Pergamon Press, 1988.

[2] C. S. Dai, *et al.*, "Effects of lead-foam grids on performance of VRLA battery," *Journal of Power Sources,* vol. 158, pp. 885-890, Aug 2006.

[3] A. Irretier and J. Banhart, "Lead and lead alloy foams," *Acta Materialia*, vol. 53, pp. 4903-4917, Oct 2005.

[4] S. M. Tabaatabaai, *et al.*, "Lead-acid batteries with foam grids," *Journal of Power Sources,* vol. 158, pp. 879-884, Aug 2006.

[5] C. S. Dai, *et al.*, "Preparation and performance of lead foam grid for negative electrode of VRLA battery," *Materials Chemistry and Physics,* vol. 99, pp. 431-436, Oct 2006.

[6] D. Linden and T. Reddy, *Handbook of Batteries* 3th ed. New York: McGraw-Hill Professional, 2001.

[7] N. Industries. *Battery seperators*. Available: http://www.kodoshi.co.jp/english/battery.html

[8] E. B. Online. (6 oct). *lead-acid storage battery: automotive-type lead-acid battery*. Available: http://www.britannica.com/EBchecked/media/19441/Construction-of-the-automotive-type-lead-acid-battery-A-storage

[9] C. A. Vincent and B. Scrosati, *Modern batteries : an introduction to electrochemical power sources*. London, New York: Arnold ; Copublished in North, Central and South America by Wiley, 1997.

[10] C. Korner and R. F. Singer, "Processing of metal foams - Challenges and opportunities," *Advanced Engineering Materials,* vol. 2, pp. 159-165, Apr 2000.

[11] T. Miyoshi, *et al.*, "ALPORAS aluminum foam: Production process, properties, and applications," *Advanced Engineering Materials,* vol. 2, pp. 179-183, Apr 2000.

[12] H.-P. Degischer and B. Kriszt, Eds., *Handbook of cellular metals: production, processing, applications* Weinheim: Wiley-VCH 2002, 398 Pages.

[13] M. F. Ashby, *et al.*, *Metal Foams: A Design Guide*: BUTTERWORTH-HEINEMANN, 2000.

[14] Y. Yamada, *et al.*, "Processing of an open-cellular AZ91 magnesium alloy with a low density of 0.05 g/cm3," *Journal of Materials Science Letters,* vol. 18, pp. 1477-1480, 1999.

[15] Y. Yamada, *et al.*, "Processing of Cellular Magnesium Materials," *Advanced Engineering Materials,* vol. 2, pp. 184-187, 2000.

[16] J. Banhart, "Manufacture, characterisation and application of cellular metals and metal foams," *Progress in Materials Science,* vol. 46, pp. 559-632, 2001.

[17] L. J. Vendra and A. Rabiei, "A study on aluminum–steel composite metal foam processed by casting," *Materials Science and Engineering: A,* vol. 465, pp. 59-67, 2007.

[18] L. Ma, *et al.*, "Cellular structure controllable aluminium foams produced by high pressure infiltration process," *Scripta Materialia,* vol. 41, pp. 785-789, 1999.

[19] C. Gaillard, *et al.*, "Processing of NaCl powders of controlled size and shape for the microstructural tailoring of aluminium foams," *Materials Science and Engineering A,* vol. 374, pp. 250-262, 2004.

[20] R. Goodall, *et al.*, "The effect of preform processing on replicated aluminium foam structure and mechanical properties," *Scripta Materialia,* vol. 54, pp. 2069-2073, 2006.

[21] S. R. Casolco, *et al.*, "Processing and mechanical behavior of Zn-Al-Cu porous alloys," *Materials Science and Engineering: A,* vol. 471, pp. 28-33, 2007.

[22] A. H. Brothers, *et al.*, "Processing and structure of open-celled amorphous metal foams," *Scripta Materialia,* vol. 52, pp. 335-339, 2005.

[23] A. Bansiddhi and D. C. Dunand, "Shape-memory NiTi foams produced by solid-state replication with NaF," *Intermetallics,* vol. 15, pp. 1612-1622, 2007.

[24] E. Castrodeza, *et al.*, "Processing of Shape Memory CuZnAl Open-cell Foam by Molten Metal Infiltration," *Journal of Materials Engineering and Performance,* vol. 18, pp. 484-489, 2009.

[25] V. Gergely and B. Clyne, "The FORMGRIP process: Foaming of reinforced metals by gas release in precursors," *Advanced Engineering Materials,* vol. 2, pp. 175-178, Apr 2000.

[26] Y. Y. Zhao, *et al.*, "Lost carbonate sintering process for manufacturing metal foams," *Scripta Materialia,* vol. 52, pp. 295-298, 2005.

[27] M. Bram, *et al.*, "High-porosity titanium, stainless steel, and superalloy parts," *Advanced Engineering Materials,* vol. 2, pp. 196-199, Apr 2000.

[28] A. Mansourighasri, *et al.*, "Processing titanium foams using tapioca starch as a space holder," *Journal of Materials Processing Technology*.

[29] N. Michailidis, *et al.*, "Compressive response of Al-foams produced via a powder sintering process based on a leachable space-holder material," *Materials Science and Engineering: A*, vol. 528, pp. 1662-1667, 2011.

[30] Q. Z. Wang, *et al.*, "Open-celled porous Cu prepared by replication of NaCl space-holders," *Materials Science and Engineering: A*, vol. 527, pp. 1275-1278, 2010.

[31] A.-E. Belhadj, *et al.*, "Elaboration and characterization of metallic foams based on tin-lead," *Materials Science and Engineering: A*, vol. 494, pp. 425-428, 2008.

[32] E. Gyenge, *et al.*, "High specific surface area, reticulated current collectors for lead-acid batteries," *Journal of Applied Electrochemistry*, vol. 32, pp. 287-295, Mar 2002.

[33] C.-S. Dai, *et al.*, "Study of influence of lead foam as negative electrode current collector material on VRLA battery charge performance," *Journal of Alloys and Compounds*, vol. 422, pp. 332-337, 2006.

[34] A. Czerwinski, *et al.*, "Electrochemical behavior of negative electrode of lead-acid cells based on reticulated vitreous carbon carrier," *Journal of Power Sources*, vol. 195, pp. 7524-7529, 2010.

[35] "DIN 50134. 2008.Testing of metallic materials — Compression test of metallic cellular materials," ed: Deutsches Institut Fur Normung E.V. (German National Standard).

[36] J. T. Yeh, *et al.*, "Semi-batch absorption and regeneration studies for CO2 capture by aqueous ammonia," *Fuel Processing Technology*, vol. 86, pp. 1533-1546, 2005.

[37] M. E. Dizlek, *et al.*, "Processing and compression testing of Ti6Al4V foams for biomedical applications," *Journal of Materials Science*, vol. 44, pp. 1512-1519, Mar 2009.

[38] H. Baker and H. Okamoto, "ASM Handbook, Volume 03 - Alloy Phase Diagrams," ed: ASM International, 1992.

[39] A. M. Alfantazi and D. Valic, "A study of copper electrowinning parameters using a statistically designed methodology," *Journal of Applied Electrochemistry*, vol. 33, pp. 217-225, 2003.

[40] G. F. Vander Voort, "ASM Handbook, Volume 09 - Metallography and Microstructures," ed: ASM International, 2004.

[41] V. R. Machavaram, *et al.*, "Fabrication of intrinsic fibre Fabry-Perot sensors in silica fibres using hydrofluoric acid etching," *Sensors and Actuators A: Physical*, vol. 138, pp. 248-260, 2007.

[42] P. Patnaik, *Handbook of Inorganic Chemicals*: McGraw-Hill 2003.

[43] I. Takishita, *et al.*, "Electrochemical Analyses of Metal Ions in HF and H2SiF6 Aqueous Solution for Recycling Silicate Glasses of Cathode-Ray Tube by Liquid-Phase Deposition," *Resources Processing*, vol. 57, pp. 114-119, 2010.

[44] A. Paul and U. Ramamurty, "Strain rate sensitivity of a closed-cell aluminum foam," *Materials Science and Engineering: A*, vol. 281, pp. 1-7, 2000.

[45] B. Jiang, *et al.*, "Effect of pore size and relative density on the mechanical properties of open cell aluminum foams," *Scripta Materialia*, vol. 56, pp. 169-172, 2007.

[46] D. R. Gaskell, *Introduction to the Thermodynamics of Materials*, 5 ed. Washington: Taylor & Francis Inc, 2008.

[47] Y. Guo, *et al.*, "Effects of H2SO4 concentrations on reduction processes of PbO layer," *Electrochimica Acta*, vol. 42, pp. 979-984, 1997.

[48] F. Beck and H. Krohn, "A Lead/graphite accumulator using aqueous hydrofluoric acid," *Journal of Power Sources*, vol. 12, pp. 9-30, 1984.

[49] A. Inayat, *et al.*, "Determining the specific surface area of ceramic foams: The tetrakaidecahedra model revisited," *Chemical Engineering Science*, vol. 66, pp. 1179-1188, 2011.

[50] M. Lacroix, *et al.*, "Pressure drop measurements and modeling on SiC foams," *Chemical Engineering Science*, vol. 62, pp. 3259-3267, 2007.

[51] M. Ashby and R. Medalist, "The mechanical properties of cellular solids," *Metallurgical and Materials Transactions A*, vol. 14, pp. 1755-1769, 1983.

[52] K. C. Chan and L. S. Xie, "Dependency of densification properties on cell topology of metal foams," *Scripta Materialia*, vol. 48, pp. 1147-1152, 2003.